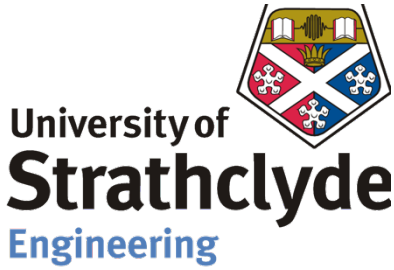

Department of Mechanical and Aerospace Engineering

An Evaluation of Material Selection for Vertical Axis Tidal Turbine Blades

Author: Grace Louise Crawford

Supervisor: Dr Olga Ganilova

A thesis submitted in partial fulfilment for the requirement of degree in

Master of Science in Sustainable Engineering: Renewable Energy Systems and the Environment

2022

202191728

Copyright Declaration

Signed:  Date: 24/08/2022

Abstract

This report details the process of building and analysing a model of a Savonius tidal turbine and how material choice affects stress distribution on the blades. This data is then compared alongside further material analysis including cost, durability, and fatigue strength to demonstrate a method of informing material choice for tidal technologies.

The model was built using Solidworks and subsequently simulated using Ansys, with sectioning taking place in Space Claim. The material of the model was then changed, and subsequent simulations of GFRP (glass fibre reinforced polymer) and CFRP (carbon fibre reinforced polymer) took place to compare these materials, as well as models consisting of Aluminium alloy and Titanium alloy. The results shown consists of global maximum equivalent stress (Von Mises stress), global maximum deformation and linearised equivalent stress along the edge of the blade. The results show that in this simulation and analysis the merits of GFRP versus CFRP are not strikingly obvious but may become clearer with future work. Aluminium and Titanium performed strongly showing lower maximum stresses on the blade than other materials chosen.

Simulation results were compared to Granta selection software analysis, which allowed for further detailed evaluation of materials according to cost versus performance and other material factors.

Acknowledgements

I would like to thank my project supervisor, Dr Ganilova, for her constant support throughout this project, whose advice and guidance proved invaluable and without which this thesis would not be half of what it has turned out to be.

A huge thanks to my partner for all his support, both within this project and out with.

Finally, a thanks to my parents, for love and support from both near and far.

Table of Contents

List of Figures

List of Tables

Nomenclature

Symbol	Description	Units
ρ	density	Kg/m3
P	Pressure	MPa
C_p	power coefficient	-
S	swept area	m^2
V	velocity	m/s
V_D	downstream velocity	m/s
V_U	upstream velocity	m/s
ω	angular velocity	Rad/s
R	rotor radius	mm
H	rotor height	mm
F	Force	N
C_D	Drag coefficient	-
A	Surface area	m^2
TSR	tip speed ratio	-

1.0 Introduction

1.1 Background

For many years now, there has been an ever-increasing demand and urgency for renewable, emission free energy across the world. This demand has resulted in a rise in research and development into a variety of renewable technologies, to combat the damage caused by fossil fuel reliant sources currently in use. Over decades it has become increasingly clear not only the damage that burning fossil fuels causes, but also in the mining and generation of such sources. While significant progress has been made in the shift to green energy, substantial developments are still to be made.

The EU has set the target of becoming "climate neutral" by 2050, requiring a 55% reduction in emissions by 2030, with multiple proposals on how this journey may look and aiming to make renewable energy more cost efficient for stakeholders and consumers [1]. Furthermore, the UK has set, in legislation, a target of achieving net zero energy by 2050, with Scotland increasing the pace of their journey to a target of 2045 [2]. Scotland is certainly at an advantage, geographically and topographically speaking, for development of renewable technology especially regarding wind, tidal and wave energy.

Ambitious targets set by Scotland have set them as a global leader in climate action, with strives made in onshore wind reaching 66% installed capacity and in offshore wind has increased capacity by 50% most recently [3]. While this is undoubtedly a hugely positive move, wind energy alone cannot solve the energy crisis. The issue that wind energy poses is that it is unpredictable, meaning that while forecasting may help, the energy produced cannot be predicted or dispatched at time of requirement [4].

One solution to this is tidal energy. Tidal energy, or hydrokinetic energy, has the capacity to make a large impact in the energy crisis, in not only feeding more energy into the grid, but also in balancing the electricity network when it depends on more unpredictable sources such as wind energy. Tidal streams are inherently predictable, which means that when utilised, they can provide a constant reliable output of energy. While estimates vary on values of potential tidal resource, a theoretical estimate of tidal Stream Energy alone is 95TWh/year in the UK [5], with tidal barrage, lagoon and wave energy also contributing significant energy as well.

Scotland in many ways is regarded at the forefront of tidal energy development, hosting the European Marine Energy Centre (EMEC), which was established in 2003. EMEC is the world's first facility for testing wave and tidal energy devices, assisted by the availability of wave and tidal resource around the Orkney Islands, with multiple test sites for development of a variety of technologies [6].

While tidal energy can theoretically provide much needed assistance and added value to the renewable energy sector, it does however have a long way to go. Arguably, the technology itself remains in infancy, with focus required to develop new ways to harness the resource potential available or improve upon current methods. In addition, there are several challenges faced by tidal turbines and other devices due to the harsh environmental and loading conditions they experience in deployment. Environmental challenges bring forth the issue of producing a turbine that will not only survive and produce energy, but while also remaining cost efficient.

1.2 Aim and Objectives

This thesis aims to investigate how material choices may affect the stress concentration and life span of tidal turbine devices, specifically the Savonius turbine, in hopes of proposing informed choices while also considering all material characteristics that will affect material feasibility. This material feasibility includes price, which remains an important factor in tidal energy development, and recyclability, which is a further issue faced by producers.

- Identification of challenges facing tidal turbine devices in the form of environmental and loading conditions
- Analysis of the affect that material choice produces on stress distribution in Savonius turbines
- Analysis of material options regarding cost and recyclability for optimising material choice
- Proposing further work to develop a more detailed analysis method considering results produced

2.0 Literature Review

This section of the report details the literature review undertaken as part of this project. It was important to review a wide range of sources to set up the beginning of the project, and devise the direction it was to take, finding gaps in knowledge and research in an ever-developing industry.

With the journey towards net zero in Scotland drawing closer, the development of new and innovative technologies to fuel energy demand becomes increasingly vital. Europe leads the way in tidal energy production [7], but the industry remains in early stages despite abundance of available tidal resources.

This section will discuss, firstly, the current state of the tidal energy industry including the current situation, where development is yet to take place, and challenges along the way. Secondly, literature on VATT or Savonius turbines will be analysed, evaluating advantages and disadvantages of this technology and where opportunity may lie in further work.

Sources used include a variety of reports on work that has been done to evaluate and analyse VATTs and their durability and performance, as well as literature discussing the current state of the tidal energy industry.

2.1 Overview of Tidal Energy

Tidal energy relies on the movement of water, powered by the gravitational pull of the sun and moon, with variations in strength of tide dependant on the volume of water flowing versus the area it must travel through, converting this kinetic energy into electricity [8]. There are three categories of tidal cycle which vary geographically: semidiurnal, diurnal, and mixed. A semidiurnal tide consists of two high tides of equal height occurring just over 12 hours apart, while a diurnal tide is characterised by a single high tide during a 24-hour period, and mixed tides again have two high tides but of unequal heights [9], shown in figure 1 [10].

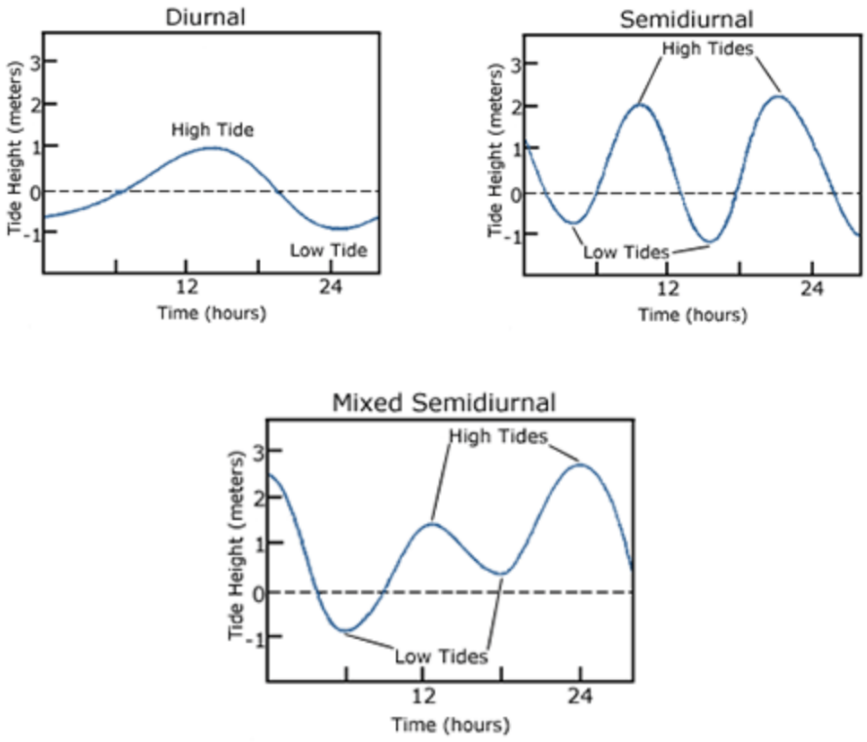

Figure 1 Tidal pattern types [10]

A common theme in almost all literature found during research makes the overarching point that tidal energy has the major advantage that it is highly predictable and reliable. In *An Up-to-Date Review of Large Marine Tidal Current Turbine Technologies*, it is stated that tidal currents are predictable for years with up to 98% accuracy [11]. Furthermore, in an article written for Marine Policy back in 2002, it is again highlighted that predictability of tidal as a resource in comparison to solar, wind and wave energy as a strong advantage [12]. Injection of renewable energy to traditional grid systems poses challenges, as these grids were not

designed to account for intermittent fluctuations in energy supply, therefore load levelling and fluctuation absorption are significant concerns for the development of renewable energy [13].

Corresponding with this theme, while predictability is stated as an advantage, almost all literature followed this with the counterpoint that the resource is largely untapped. This theme ranges from sources that have been written as recently as this year, to sources 20 years ago. While development has been made, and tidal energy has developed greatly throughout the 21st century, a common statement is that potential remains largely untapped, and technology in its infancy. Multiple reasons are posed to answer the question of why this is the case, across various sources. Esteban and Leary pose that while there is estimated to be a global potential of around 3000GW of tidal energy, only 3% or less of this is suitable to be harnessed, located in areas that are appropriate for electricity generation [13]. Such areas optimised for tidal turbine energy production are often posed as areas where the tide is already constrained by the topography of the seabed and surrounding land, such as between islands where the current is accelerated to 2.5m/s or above, which makes it easier to produce enough energy to become cost effective [14].

Furthermore, while tidal turbines often resemble their land born counterparts, often the amount of energy they can harvest is higher. The power produced is dependent on the density of the surrounding medium, the coefficient of power, the swept area of the turbine and the velocity of the current, equation 1 shows the power equation for a horizontal axis turbine [15].

Equation 1

$$P = \frac{1}{2}\rho C_p S V^3$$

Where P is the power of the turbine, ρ is the density of the surrounding medium, S is the swept area of the turbine, V is the velocity of the medium and C_p is the power coefficient.

Importantly, due to this equation, tidal turbines can produce more energy with an equal or smaller swept area than wind turbines, due to the increase in density of the surrounding medium.

The power coefficient of the turbine is dependent on both the upstream and downstream velocities, as shown in equation 2 [16].

Equation 2

$$C_p = \frac{1}{2}\left(1 - \frac{V_D}{V_U}\right)^2 (1 + \frac{V_D}{V_U})$$

Where V_D denotes the downstream velocity and V_U denotes the upstream velocity.

Furthermore, the tip-speed-ratio (TSR) of the turbine is dimensionless factor, shown in equation 3 [16].

Equation 3

$$TSR = \frac{V_D}{V_U} = \frac{\omega R}{V_U}$$

Where R is the radius of the rotor and ω is the angular velocity at which the rotor is travelling. The relationship between the TSR and the power coefficient can be seen in figure 2.

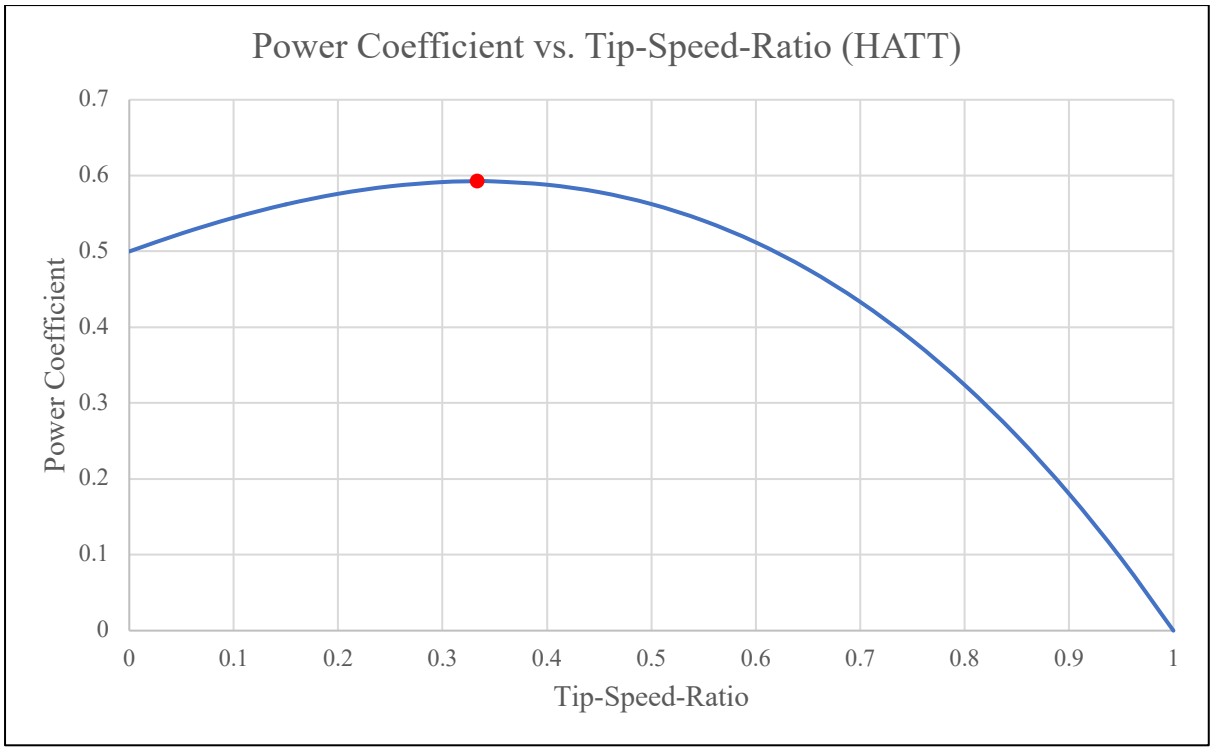

Figure 2 Relationship between power coefficient and TSR

The theoretical maximum power coefficient is marked in red on the graph, which lies when the TSR is equal to 1/3, with C_p equal to 0.59.

2.2 Types of Tidal Turbine

There are a variety of different technologies employed to harness energy from the tides. This section will give details on horizontal and vertical axis turbines and their relative advantages and disadvantages.

2.2.1 Horizontal and Vertical Axis

Horizontal and vertical axis turbines use blades or hydrofoils similar to wind turbines, with axes either perpendicular or parallel to the flow of water. Horizontal axis turbines are more common than vertical axis, with horizontal axis turbines making up 76% of turbines, and vertical making only 12% [17]. Figure 3 shows a comparison of HATT and VATT examples.

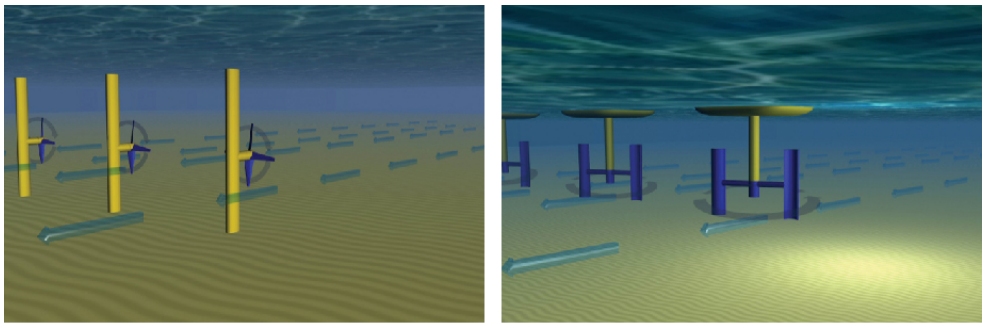

(a) HATT (b) VATT

Figure 3 Horizontal and vertical axis turbine examples (Source: Aquaret)

There are multiple subsets of both horizontal and vertical axis turbines, with variations in driving mechanism especially affected by the design of the blades attached. While some turbines operate driven by lift, others operate via drag.

Considering drag driven turbines, the blades hinder the movement of water. The impact resistance, therefore, from this movement is converted to rotational driving force and axial thrust, producing rotation of the turbine [18]. Figure 4 shows a diagram of a drag driven tidal turbine [18].

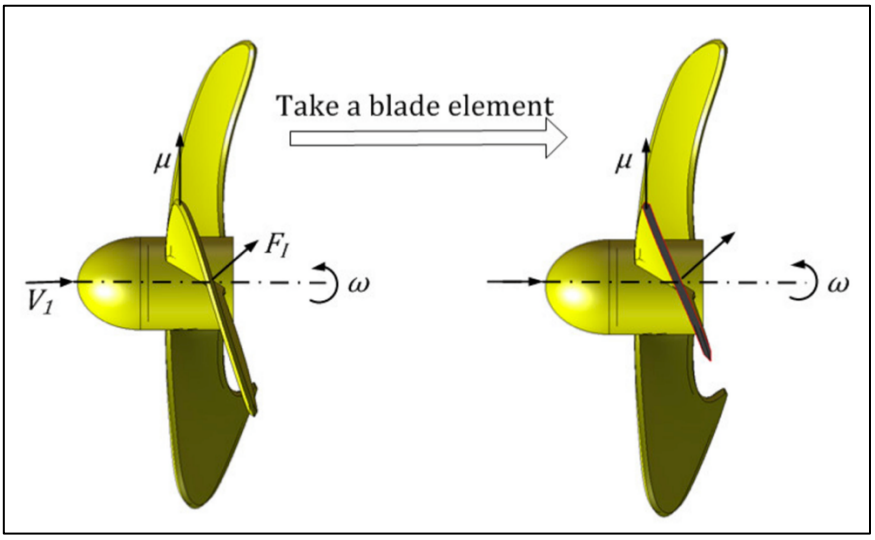

Figure 4 Diagram of a drag driven tidal turbine example (source: [18])

Across multiple literature sources there have been examples given of advantages and disadvantages given for vertical and horizontal axis turbines. In most literature, it is only vertical axis turbines that are referred to when considering drag based configurations, however, horizontal axis turbines can also be classified as such depending on composition. Therefore, in many reports considered, the statements made make sweeping statements that disadvantages only relate to vertical axis turbines, where this would be better explained as drag based turbines.

Table 1 shows a summary of advantages and disadvantages for HATT and VATT.

Table 1 Advantages and disadvantages of HATT and VATT

HATT	
Advantages	**Disadvantages**
High power output [19]	More challenging installation especially due to generator placement
High efficiency [19]	Turbulence wake production causing tip losses [20]
VATT	
Advantages	**Disadvantages**
Relatively simple design allowing for inexpensive manufacture [21]	Lower efficiency [22]

Generator placement above the water allows for easier instalment and maintenance [21]	Low starting torque [19]
Can operate in any flow direction	
More compact than HATT	

When considering disadvantages of drag driven turbines or VATTs a recurring theme is that in comparison to their lift driven counterparts the start-up torque is significantly lower (find the ref for this).

A significant advantage of vertical axis turbines that is often used to mitigate disadvantages of the technology is that the configuration allows for other components such as the generator to be placed out of the water, above the blades and shaft themselves allowing for, firstly, an easier and cheaper instalment process. This assists in lengthening the lifetime of the turbine, and eases issues that can be caused by having to seal electrical components. In addition to the lifespan, this also eases maintenance of the turbine. If it possible to position most components out of the water, they are easier reached for survey and maintenance.

Advantages of horizontal axis turbines are stated such as having a higher efficiency alongside higher power output in comparison to VATTs.

It is clear from literature that both horizontal and vertical axis turbines have both desirable and less desirable traits. When choosing between either configuration it becomes a choice between expense, ease of manufacture and installation, and consequent power output. While horizontal axis turbines currently take precedence over vertical axis turbines due to higher power output, it is worth further research and development into VATTs.

2.3 Savonius Turbine

The Savonius turbine is a type of VATT, one of a few subsets of the technology. It is often posed that the shape of the blades on a Savonius turbine is comparable to that of an anemometer, used to measure wind speed. This type of turbine is definitively drag based, operating by disrupting the flow of the water, turning that resistance into rotational movement. The varying compositions of vertical axis tidal turbines can be seen in figure 5 [23].

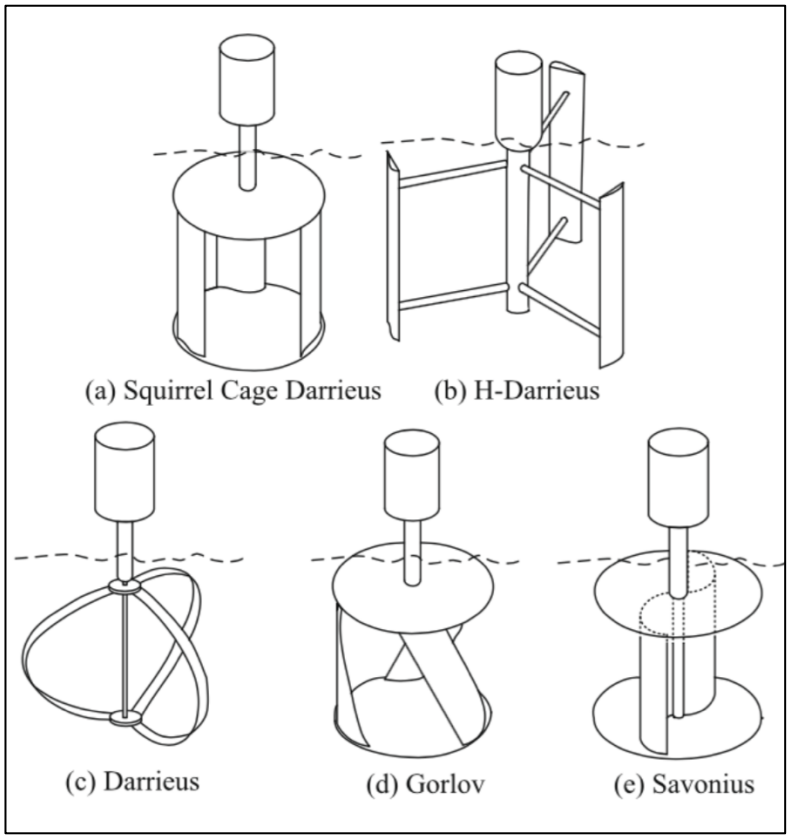

Figure 5 Example configurations of vertical axis tidal turbines [23]

From above, the Savonius turbine blades are often described as showing an S shape, and can be designed using two, three or four blades. As mentioned in section 2.2.1, an advantage of this turbine is that the generator and other components can be housed above the water. The Savonius turbine is a prominent choice for vertical axis turbines, developed by Finnish engineer S. Savonius in 1931 initially for wind applications, with experimental analysis showing the turbine to reach maximum power coefficients between 0.15 to 0.35 [24].

With advantages of this turbine type including high starting torque, low manufacturing costs, low noise emission and low rotational speed, the Savonius hydrokinetic turbine is an attractive choice for developers [25]. Despite these advantages, challenges faced with this design is such as low efficiency and large variation of static torque [26].

For Savonius rotors, the mechanical power is dependent on similar factors as previously mentioned in section 2.1, but with the height of the rotor replacing the swept area. Equation 4 shows the general equation [27].

Equation 4

$$P = C_P \times \rho \times R \times H \times \boldsymbol{V}^3$$

Where P denotes the mechanical power, C_P is the power coefficient, ρ is the density of the surrounding medium, R is the radius of the rotor, H is the height of the rotor and **V is the upstream velocity of the surrounding medium.**

The tip speed ratio for Savonius rotors remains the same as previously mentioned in section 2.1.

The Savonius turbine was chosen to move forward with this project for further analysis, due to current strides in the production of the technology, with a different approach than previous development of tidal turbines in the form of horizontal axis. For example, there has been development of arrays formed of Savonius turbines assisted by their compact size, which allows multiple to be packed into small areas [28], creating a high concentration of several turbines able to produce relatively significant amounts of energy while minimising the amount of space taken up on the sea floor.

2.4 Challenges Facing Tidal Turbines

There are a significant number of challenges facing tidal turbines, both affecting life span and energy production. Deployed in a harsh environment, tidal turbines experience highly loads than wind turbines. Even though tides move much slower than wind, the density of the medium produces stronger forces and loads on the components. These loads are often fluctuating and cyclical [29], meaning that survival of blades, bearings and other machinery is more challenging. Due to such loads and the surrounding environment, often the lifespan of tidal turbines falls short of schedules created by manufacturers [30]. In addition to loading conditions, the importance of the materials capability to survive in salt or fresh water for extended periods of time, many years in fact, is vital.

One such challenge to be faced is fatigue. Due to the unsteady and cyclical nature of the loads experienced, fatigue life is a major concern for tidal turbines. Work has been carried out in previous years to evaluate the magnitude of the effect this may have, and the level of sensitivity each component may have, alongside driving factors. In studies carried out such as McCann in 2007 [31], where site conditions were created using a variety of fixed flow speeds, turbulence

intensities and wave conditions. This study found that fatigue life was highly sensitive to both turbulence and wave conditions. However, it is also important to note that while researching this area, there are studies that have been carried out, there are also a significant number of studies to be started. While testing and modelling has been able to determine the driving forces in fatigue, there are gaps in knowledge as to how this may affect stress distributions and blade bending, with research gaps in areas such as adapting blade material to combat this.

Furthermore, cavitation always poses a risk to lifespan. Improvements to blades in response to cavitation is an area that has not yet been fully researched or understood. Cavitation is the result of the increasing velocity of a fluid which causes a decrease in hydrostatic pressure, in accordance with Bernoulli's principle. When this pressure falls below the vapour pressure of the fluid, vapour bubbles are created and collapse at a high rate [32]. This therefore can produce pitting and corrosion to components, as well as an increase in vibration and fatigue, often causing the material to fail, in conjunction with corrosion [33].

While there has been research carried out to investigate improvement to blade design and material choices, this area is largely unknown currently. Tidal turbine blades are often produced using composite materials like wind turbines, with glass fibre reinforced polymers most favoured due to high specific strength and stiffness, resistance to corrosion and reasonable cost. While there are benefits to using such materials, studies have shown that they become moisture saturated early in their installation [34]. While cost reduction and management is vital for companies introducing tidal turbines to the energy industry, material choice becomes a challenge between survival and expense.

Vibration in turbines can pose risks to durability. This factor is inherently connected to the challenge of difficult maintenance and monitoring. In recent years, there have been a few studies carried out to develop monitoring systems for tidal turbines, or systems to assist in predicting vibration in turbines. There are papers such as *Galloway et al 2020,* which proposes a condition monitoring system from monitoring data with low sample rates in collaboration with developers, aiming to assist in predicting faults and failures in tidal turbines. While this produced the beginning stages of a monitoring system, further work is required to develop this system as well as research into predicting modes of failure [35].

Furthermore, it is important to note work that is currently being done to investigate recycling of traditional composites such as glass fibre that is often used for production of tidal and wind turbines. These materials are known to be difficult to break down and form a source of pollution

when no longer in use, with estimates predicting wind turbine waste increasing from approximately 400,000 tonnes/year in 2030 to almost 2 million tonnes by 2050 [36].

With these challenges in mind, it was decided that the project would focus upon the durability of the materials regarding loading conditions and forces the blades are subject to, as well as considering corrosion resistance and recyclability.

3.0 Method

This section details the modelling work and subsequent analysis undertaken to determine the effects of material choice on stress distributions in Savonius tidal turbine blades, to extend the lifespan and reduce opportunity for failure or cracking in components.

The model created was in part reproduced from information from two different research reports written. The reason for this was to begin the modelling and analysis at a point where it could be verified without further work afterwards, meaning that the simulation results verify the model itself before changes are made. The report used for modelling verification *Numerical investigation of hydraulic load and stress induced in Savonius hydrokinetic turbine with the effects of augmentation techniques through fluid-structure interaction analysis* by Dinesh Kumar and Shibayan Sarkar from the Department of Mechanical Engineering (ISM) provided dimensions, material choices and conditions for the simulation. Calculation of forces was assisted by literature alongside further research into the method, which is referenced in the relevant sections.

The model was firstly built in Solidworks, allowing it to be imported into Space Claim. This then allows the model to be split and partitioned to allow for meshing and finally, simulation using Ansys software. Following this, changes were made to the model by adapting the construction material, with chosen materials according to literature and GRANTA material selection software.

3.1 Building the model in Solidworks

As previously mentioned, the geometry of the model was taken from Kumar and Sarkar (2016), with figure 6 showing the dimensions used [37].

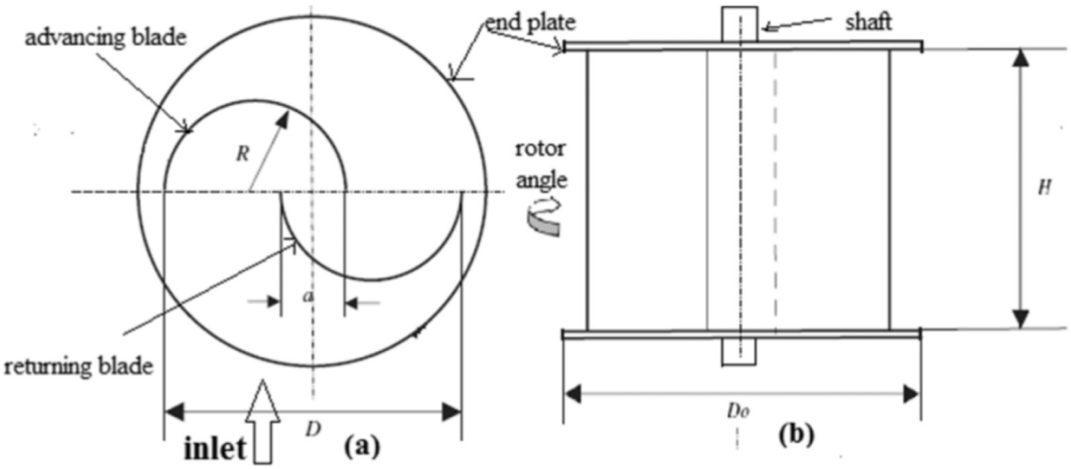

Figure 6 Dimension diagram given in Kumar and Sarkar [20]

The dimensions of the model are as follows:

$$D = 245mm \quad H = 245mm \quad D_o = 269.5mm \quad a = 36.75mm$$

$$blade\ thickness = 3mm \quad shaft\ diameter = 30mm \quad end\ plate\ thickness = 10mm$$

These dimensions were utilised to recreate this model in Solidworks, as shown in figure 7.

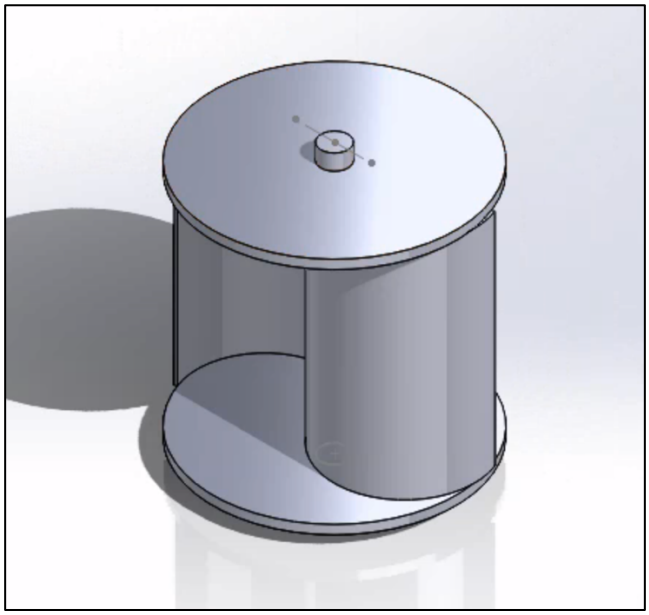

Figure 7 Isometric view of model created in Solidworks

In figures 8 and 9 below, further details of the model can be seen. Shown in figure 8, the top view demonstrates the dimensions from figure 6.

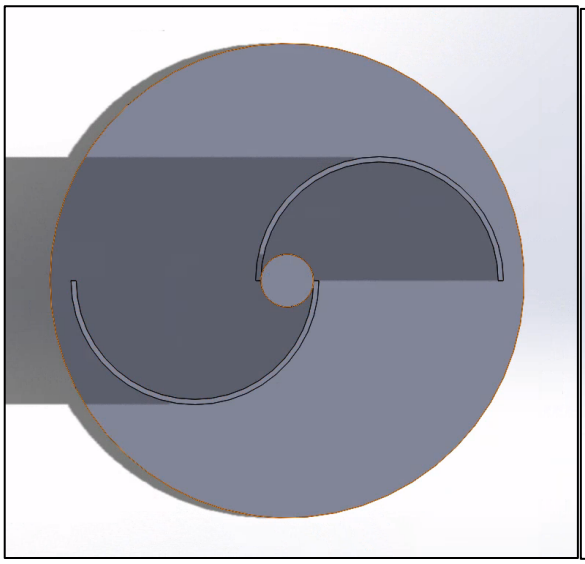

Figure 8 Top view of Savonius model created in Solidworks

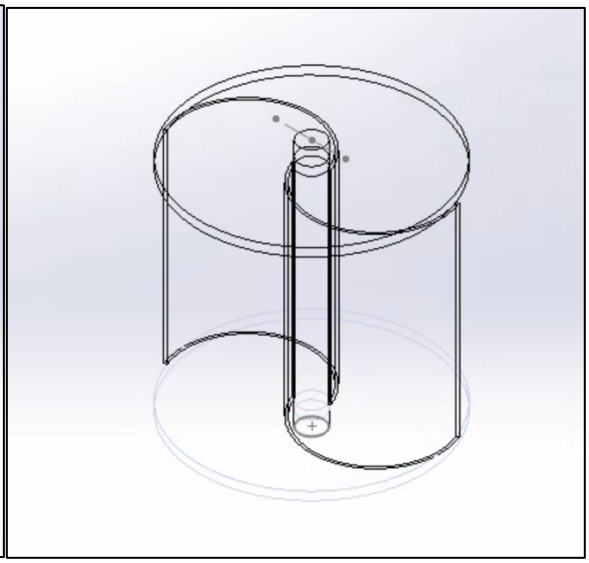

Figure 9 Transparent view of whole model

3.2 Partitioning and Meshing for Ansys

Following from the creation of the model in Solidworks, it was necessary to prepare the model for simulation. In order to do this, the model was loaded into Space Claim, where the model was partitioned to assist in meshing and simulating.

It is vital when inserting a model into simulation software that it is suitably partitioned, or broken up into smaller pieces, to assist with not only accuracy of results and meshing, but also to reduce CPU time taken for the simulation to be carried out. Areas of specific interest are broken up and constricted so that the mesh can be structured and fine, even if such areas consist of complex or curved geometry.

Firstly, it was decided that to create an organised mesh around the blades, they were to be split into 4 sections each. This included splitting the blades down the middle, to create two thinner sections, and to split the blades down the top of their curve to assist in the meshing of the curved area. This partitioning can be seen in figures 10 below.

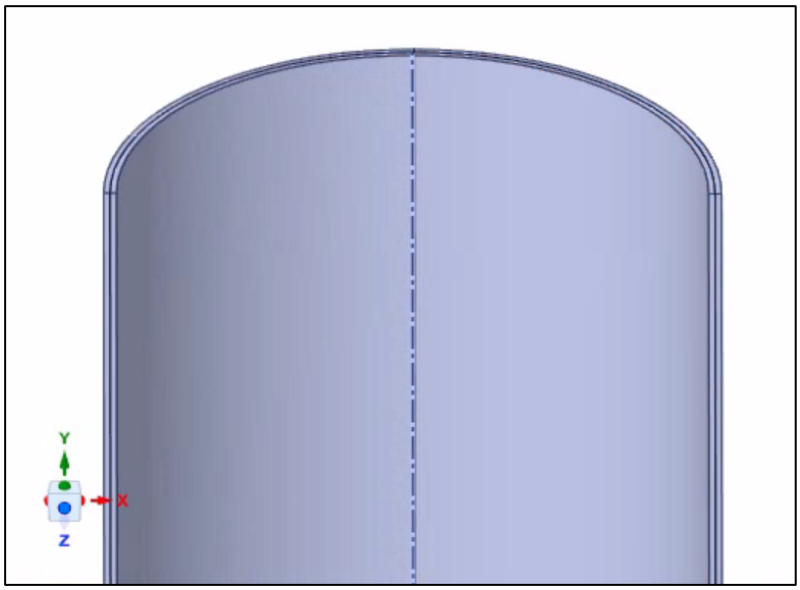

Figure 10 Blade partitioning in Space Claim into 4 sections

Furthermore, transition zones were partitioned in the areas where the blades meet the end plates. This is to assist the software in creating a neat mesh around these areas, which will also further assist in accuracy of simulation results. These transitions consist of three zones, the middle being directly where the blade meets the end plate, and a further two zones on either side of this with a width of 3mm, shown in figure 11.

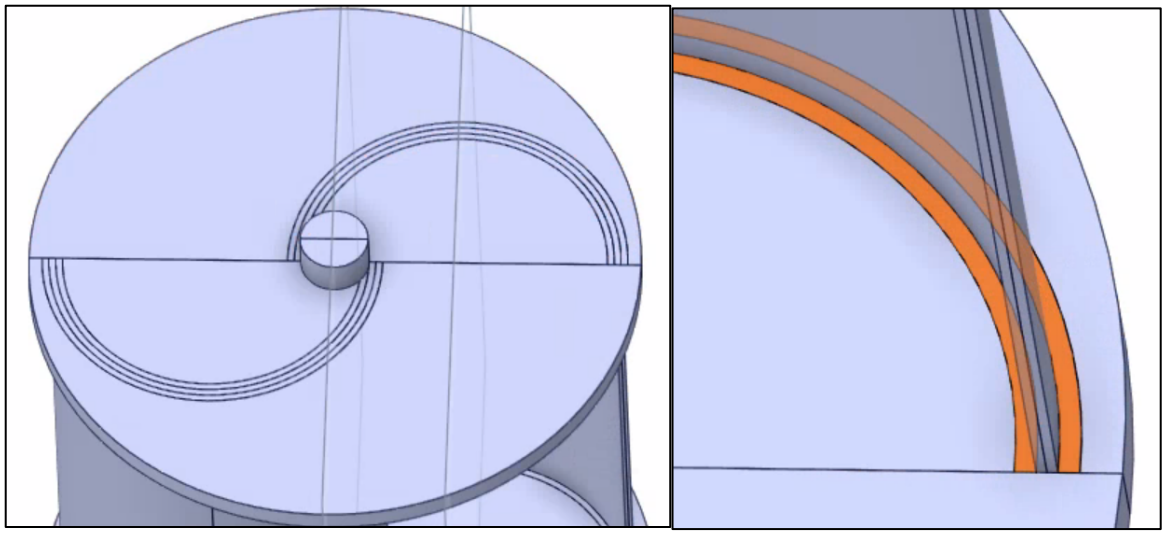

Figure 11 Transition zones partitioned where blade contacts the endplates

Finally, the shaft in the centre of the model was split in two, vertically, shown in figure 12. This assists in further organising the mesh and allowing for more accurate values.

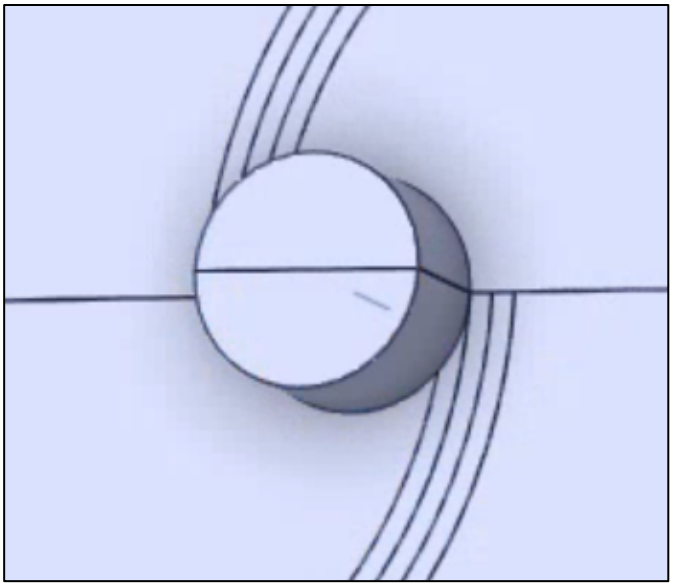

Figure 12 Shaft partitioning vertically down the centre

Utilising the partitions on the blades, seed sizes were implemented to constrict the size of elements further on this mesh, meaning that the mesh can remain regularly distributed across the area without creating areas of looser mesh due to geometry.

With the model fully partitioned and seeded where necessary, the model was ready to be meshed for simulation. Due to decisions made in this process, the blades and their surrounding areas have a significantly finer mesh than the rest of the model, due to being the areas with the highest expected stress and therefore requiring the most detail in simulation results.

The order of meshing remained constant throughout the study, as is best practice for maintaining a well-structured mesh. Firstly, all blade sections were meshed first, as shown in figure 13.

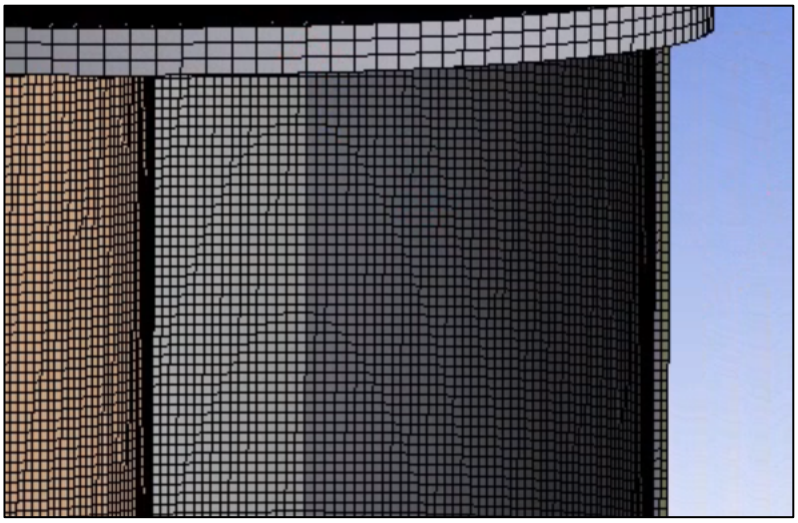

Figure 13 Fully meshed blade

Afterwards, the transition zones were meshed, with the middle of the three meshed first and the outside two following afterwards. Figure 14 shows the meshed transition zones.

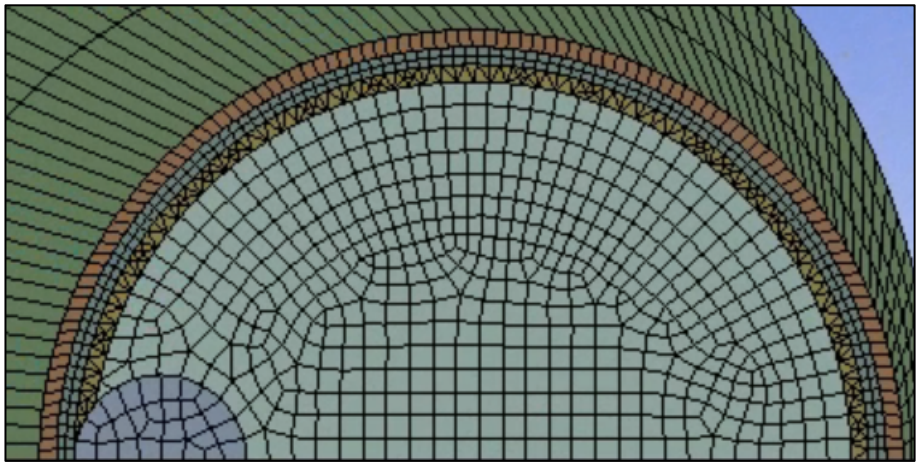

Figure 14 Transition zone mesh

Finally, the rest of the model body was meshed, with the whole model after meshing shown in figure 15.

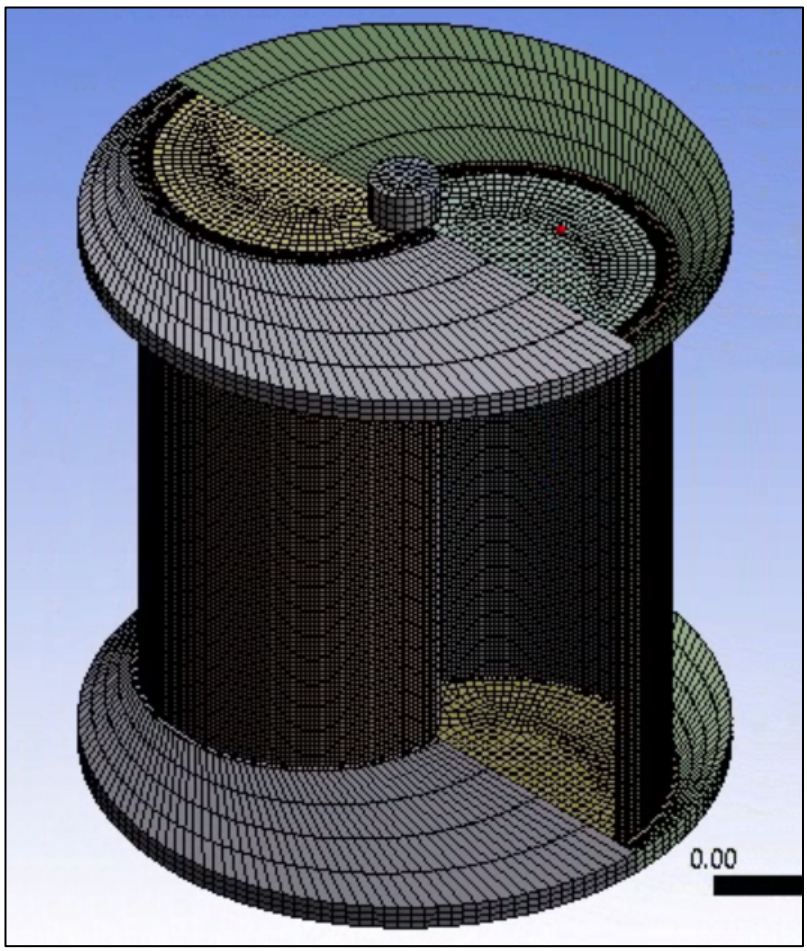

Figure 15 Fully meshed model in Ansys

With the model completely meshed, it was then possible to move on to further stages of the simulation process, such as adding the conditions it would be subject to.

3.3 Forces and Boundary Conditions

This section details the boundary conditions and forces applied to the model prior to simulation.

Firstly, boundary conditions are added such that the shaft remains fixed, this is achieved by adding a fixed support to either end of the shaft. The simulation carried out is a static structural simulation, meaning no dynamic loads will affect the model. When the model is added to space claim, it becomes one solid structure, meaning that since the shaft is a fixed support, the model

will not rotate when force is applied. As this is the case, the blades and endplates are subject to deformation due to stress. The fixed support boundary condition added to the shaft can be seen in figure 16.

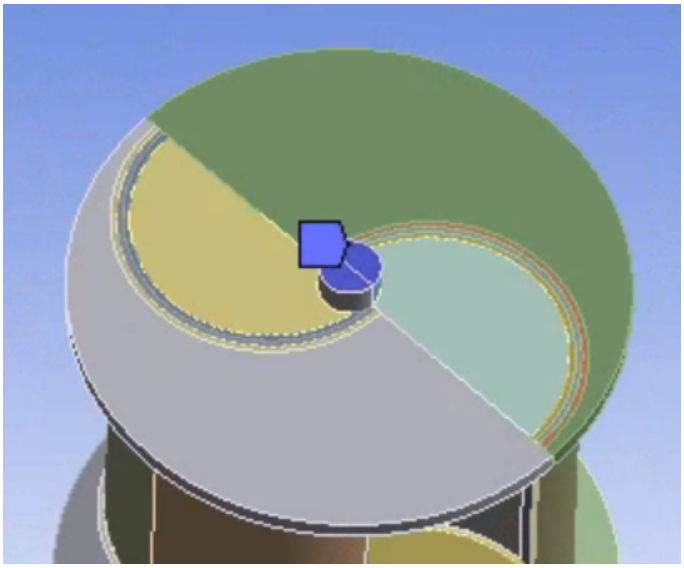

Figure 16 Boundary condition applied to the shaft, fixed support

In the report used for verification, the forces were taken from CFD calculations and imported in to Ansys. The reproduction of such results was out of scope for this project and therefore, environmental conditions were taken from the report and simplified forces were calculated. The forces applied to the model are dependent on a variety of parameters. Geometry was considered, which affects the drag coefficient and therefore the forces exerted on each blade. It was decided that the forces would be applied to only the blades, as other reaction forces due to drag would be much lower and therefore negligible for this simulation.

Furthermore, the environmental conditions such as density and velocity of the water affect the force applied, and these were taken from the most extreme example in the report as a starting point for calculation.

The calculations for the forces to be applied were as follows [38].

Equation 5

$$F = C_D(0.5 \times \rho \times A \times V^2)$$

Where F is the force, C_D is the drag coefficient dependant on the geometry of the object, ρ is the density of the water, which in this calculation was 998.2 kg/m3 according to the report used for reference, A is the surface area, and **V is the velocity of the water flow**.

The surface area calculation based on the geometry of a single blade was as follows.

Equation 6

$$A = \frac{\pi}{2} \times (0.14088)^2 \times 245 = 0.054\ m2$$

The drag coefficient is a constant defined by the geometry of the blade and was taken from literature. The drag coefficient varies depending on the orientation of the shape used for the blades, and therefore, two separate calculations were used.

The drag coefficients used are shown in figure 17. [39]

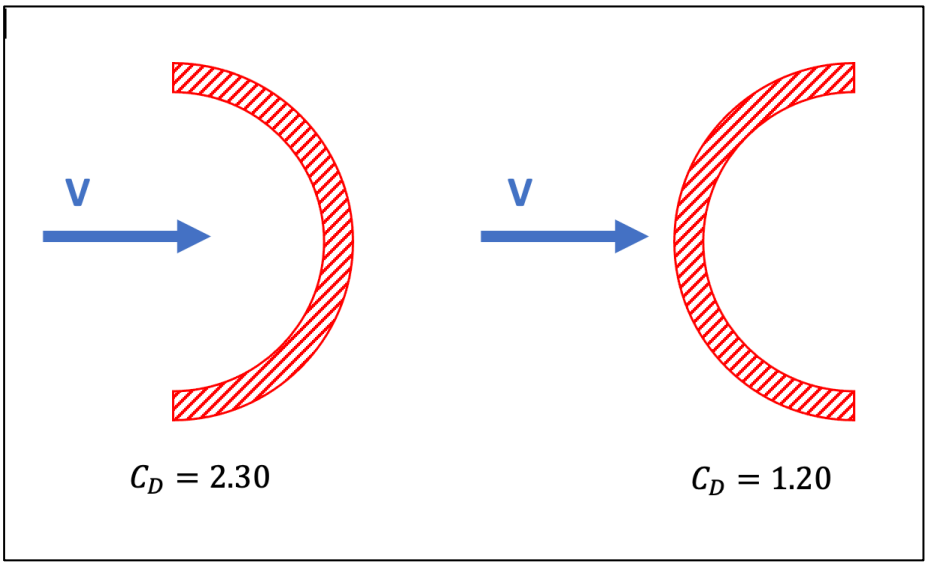

Figure 17 Drag coefficient values dependant on geometry, V indicates velocity and direction of water

Therefore, the following factors for force calculations were:

V = 4m/s $\quad \rho = 998.2 kg/m^3 \quad$ A = 0.054 m^2

Therefore, the forces applied to the model in Ansys were calculated as shown in equation 7 and 8.

Equation 7

$$F = 2.30(0.5 \times 998.2 \times 0.054 \times 16) = 991.81\ N$$

Equation 8

$$F = 1.20(0.5 \times 998.2 \times 0.054 \times 16) = 517.467\ N$$

A graph of force exerted versus the velocity of water, on both of the orientations of the blade, was created using equation 5, shown in figure 18.

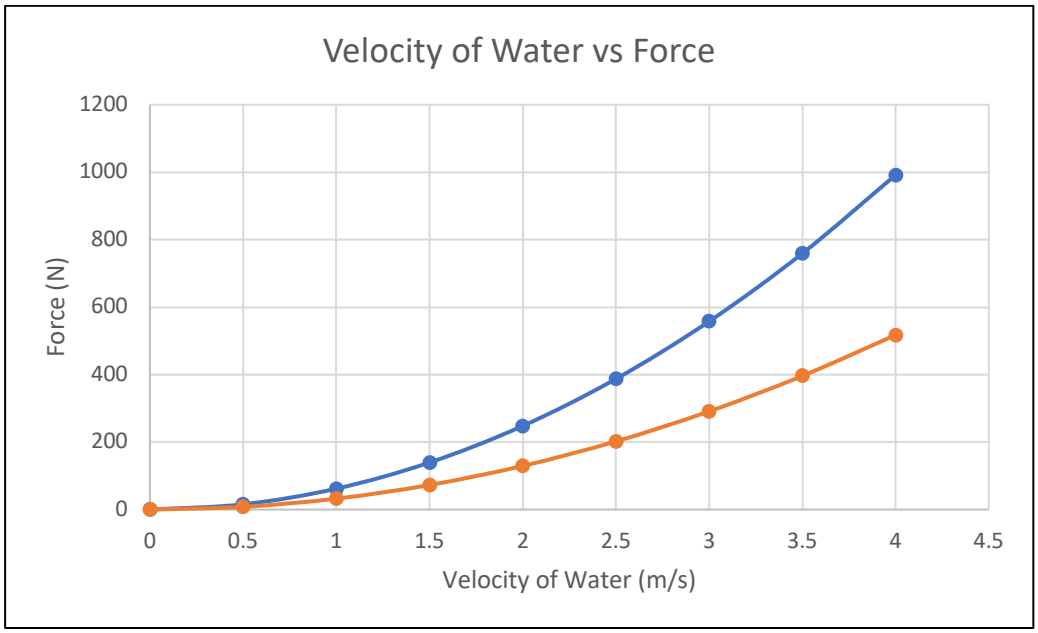

Figure 18 Chart of relationship between water velocity and force exerted

Finally, as a simplification, the drag forces on the rear of the blades caused by water resistance were assumed to be much smaller than the drag forces calculated above. This is due to the speed of the blades travelling though the water being much smaller than the speed of the water contacting the blades. Therefore, these reaction forces were assumed to be negligible, and it was only the calculated forces that were applied to the front side of the blades.

3.4 Simulation

To begin the process of simulation after the addition of the mesh, boundary conditions and forces that the model was subject to, it was necessary to carry out a mesh convergence study. The purpose of this is to deduce how fine the mesh needs to be to remain accurate, while also considering CPU time. To do so the forces remained constant throughout and the only changes made were to mesh size, which were gradually made finer, the simulation run, and the maximum stress recorded.

The outcome of the mesh convergence study can be seen below in figure 19.

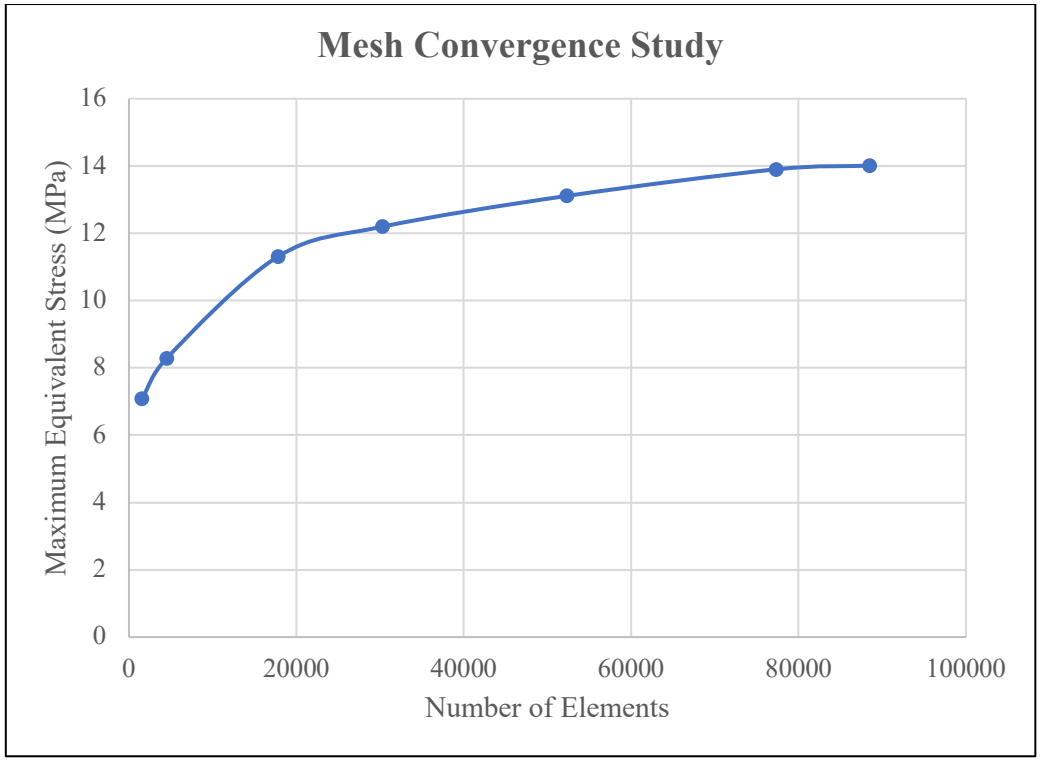

Figure 19 Mesh convergence study: maximum equivalent stress versus number of elements

During the study, the final data point that can be seen on the graph, with 88501 elements, the CPU time for the simulation was significantly higher than all other simulation runs, meaning that this mesh size was not sustainable. Therefore, it was decided to continue with the mesh size shown in the second highest data point, with 77325 elements. This mesh size, while taking a relatively long time to compute and run, gave satisfactorily accurate results. This included seed sizes of 2mm along the blade edges, and a default element size of 4mm for the rest of the model body. Examples of coarser meshes used for this study, as well as a table of element numbers versus maximum recorded equivalent stresses can be found in Appendix 1.

A path was added along the edge of one of the blades, as shown in figure 20.

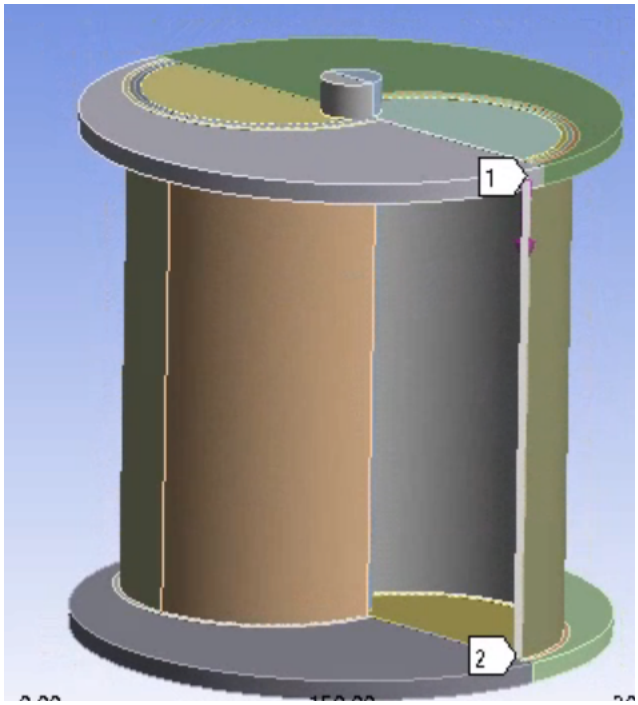

Figure 20 Path along edge of blade, from point 1 to 2

The purpose of the path was to highlight the stress along this line, with this area being chosen due to being the point at which the highest stress was recorded in the first simulation run. This path allowed a graph to be produced of the stress from point 1 to 2, meaning that the stresses along this line when changes were made were more easily comparable.

The outputs of the simulation were therefore chosen as total deformation, equivalent stress (Von Mises stress) and linearized stress along the path.

4.0 Material Analysis (Granta)

This section details the analysis of changes made to the model to consider reducing the maximum stress on the blades of the turbine, to extend the lifespan and reduce risk of fatigue or crack failure. Furthermore, material analysis was carried out to inspect the characteristics of the material that a static structural Ansys analysis could not provide.

The process of defining materials to consider on further analysis was a combination of literature review and use of GRANTA software.

It was important to consider a variety of factors when choosing materials, while a material may improve the lifespan of the turbine it may also come with an increase in cost and in manufacturing difficulty. This was considered when choosing materials and can be seen in graphs produced.

In the process of material analysis using GRANTA, the database used in particular was Level 2 Sustainability. Limits were added to this database to begin narrowing the search for material choices for analysis. The first of which included the durability of the material in water, both fresh and salt, which were narrowed to excellent performance only. Furthermore, graphs were created to demonstrate the differences between materials that qualify under such limitations, to determine optimum material choices for further simulation and investigation.

It was also important to consider while conducting this analysis, the price of the materials being considered. While material performance and durability were of the highest importance, the importance of price cannot be discounted as this remains a considerable factor in the design and production of tidal turbines.

4.1 Material Simulation

The first material chosen to model was GFRP (glass fibre reinforced polymer). This was because currently, tidal turbine material choice tends to favour GFRP, considering significant similarities in design approach in comparison with wind turbines.

GFRP is commonly used in tidal and wind turbine blades thanks to its high strength and stiffness, as well as relatively low cost in comparison to other material options [40]. However, it is also emphasised in literature such as *Marine Application of Fibre Reinforced Composites: A Review, F Rubino et al (2020),* that GFRP is often chosen due to a trade-off between structural properties and cost, where CFRP (carbon fibre reinforced polymers) offer higher performance and lower weight and the use of GFRP sets a limit on the dimensions of blades that can be produced due to the materials durability under the extreme working conditions it is subject to.

For the first adapted simulation it was decided that GFRP would be used as the material for the model. The material properties of GFRP were taken from Granta software and added to the Ansys simulation, and are shown in figure 21, with the minimum values taken from each range.

Mechanical properties					
Young's modulus	ⓘ	* 21	-	21.8	GPa
Shear modulus	ⓘ	* 7.99	-	8.29	GPa
Bulk modulus	ⓘ	* 6.8	-	7.85	GPa
Poisson's ratio	ⓘ	* 0.314	-	0.315	
Yield strength (elastic limit)	ⓘ	* 207	-	304	MPa
Tensile strength	ⓘ	* 207	-	304	MPa
Compressive strength	ⓘ	* 207	-	257	MPa
Elongation	ⓘ	* 0.85	-	0.95	% strain
Hardness - Vickers	ⓘ	* 10.8	-	21.5	HV
Fatigue strength at 10^7 cycles	ⓘ	* 41.3	-	91.1	MPa
Fracture toughness	ⓘ	* 19.3	-	31	MPa.m^0.5
Mechanical loss coefficient (tan delta)	ⓘ	* 0.0028	-	0.0029	

Figure 21 Mechanical material properties of GFRP (source: Granta EduPack 2021)

For purposes of comparison, CFRP, was also added for analysis. Significant literature in current years aims to analyse the advantages of producing tidal turbine blades out of CFRP, such as Alam *et al,* with the main drawbacks being that it is a more expensive material [41]. The material properties of CFRP are shown in figure 22.

Mechanical properties					
Young's modulus	ⓘ	69	-	150	GPa
Shear modulus	ⓘ	28	-	60	GPa
Bulk modulus	ⓘ	43	-	80	GPa
Poisson's ratio	ⓘ	* 0.305	-	0.307	
Yield strength (elastic limit)	ⓘ	550	-	1.05e3	MPa
Tensile strength	ⓘ	550	-	1.05e3	MPa
Compressive strength	ⓘ	440	-	840	MPa
Elongation	ⓘ	* 0.32	-	0.35	% strain
Hardness - Vickers	ⓘ	* 10.8	-	21.5	HV
Fatigue strength at 10^7 cycles	ⓘ	* 150	-	300	MPa
Fracture toughness	ⓘ	* 6.12	-	20	MPa.m^0.5
Mechanical loss coefficient (tan delta)	ⓘ	* 0.0014	-	0.0033	

Figure 22 Mechanical material properties of CFRP (source: Granta EduPack 2021)

From these figures it can be seen that the Young's modulus of CFRP is significantly higher than that of GFRP, alongside significantly higher yield and tensile strengths, meaning it was expected that under loading conditions CFRP would show stronger performance than GFRP.

To act as a further comparison to the polymers previously mentioned, titanium alloy was also added for analysis. Figure 23 shows the mechanical material properties of titanium alloy.

Mechanical properties					
Young's modulus		110	-	120	GPa
Shear modulus		38	-	45	GPa
Bulk modulus		110	-	120	GPa
Poisson's ratio		0.33	-	0.35	
Yield strength (elastic limit)		701	-	1.09e3	MPa
Tensile strength		763	-	1.19e3	MPa
Compressive strength		* 680	-	1.15e3	MPa
Elongation		6	-	20	% strain
Hardness - Vickers		223	-	373	HV
Fatigue strength at 10^7 cycles		* 412	-	636	MPa
Fracture toughness		51.3	-	86.1	MPa.m^0.5
Mechanical loss coefficient (tan delta)		* 0.001	-	0.002	

Figure 23 Mechanical material properties of Titanium alloy (source: Granta EduPack 2021)

Titanium alloy provides highly desirable material characteristics in environments of high stress and loading and can be used as an exemplar choice for baseline comparison in the simulation section of this project.

Finally, aluminium alloy was added for simulation as another comparison for strong mechanical performance, mechanical material properties are shown in figure 24.

Mechanical properties					
Young's modulus		69	-	74	GPa
Shear modulus		25	-	28	GPa
Bulk modulus		66	-	77	GPa
Poisson's ratio		0.32	-	0.34	
Yield strength (elastic limit)		65.1	-	252	MPa
Tensile strength		151	-	323	MPa
Compressive strength		* 65.1	-	264	MPa
Elongation		4.3	-	23	% strain
Hardness - Vickers		37.8	-	98.3	HV
Fatigue strength at 10^7 cycles		* 61.7	-	150	MPa
Fracture toughness		* 27	-	37	MPa.m^0.5
Mechanical loss coefficient (tan delta)		0.0011			

Figure 24 Mechanical material properties of Aluminium alloy (source: Granta EduPack 2021)

5.0 Results

5.1 Ansys Results

After building the model and adding all parameters, the simulation was run using the reference material, steel. The first set of results came from the steel analysis, which was the same material used in the reference report. Figure 25 shows the results for equivalent stress on the whole model, with the point of maximum equivalent stress labelled.

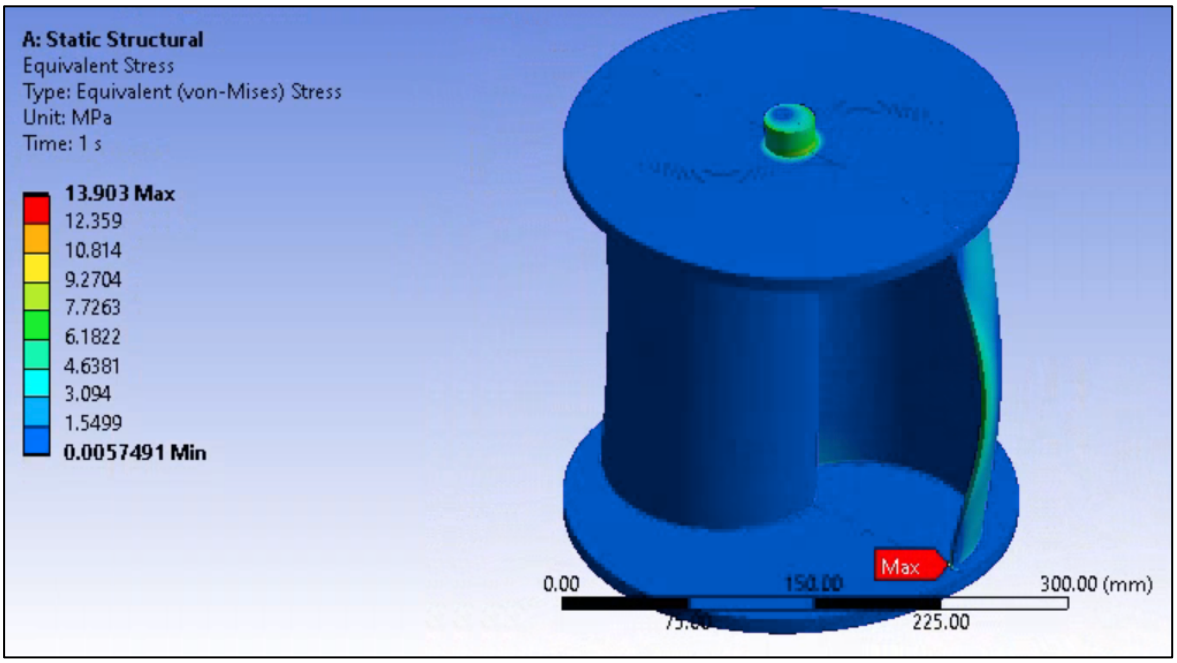

Figure 25 Equivalent stress distribution on unchanged model with maximum stress shown on bottom of blade

As can be seen from the figure, the maximum stress is at the bottom of the blade, where it meets the endplate, and reaches a maximum value of 13.903 MPa.

The total global deformation of the model is shown in figure 26, with the maximum labelled.

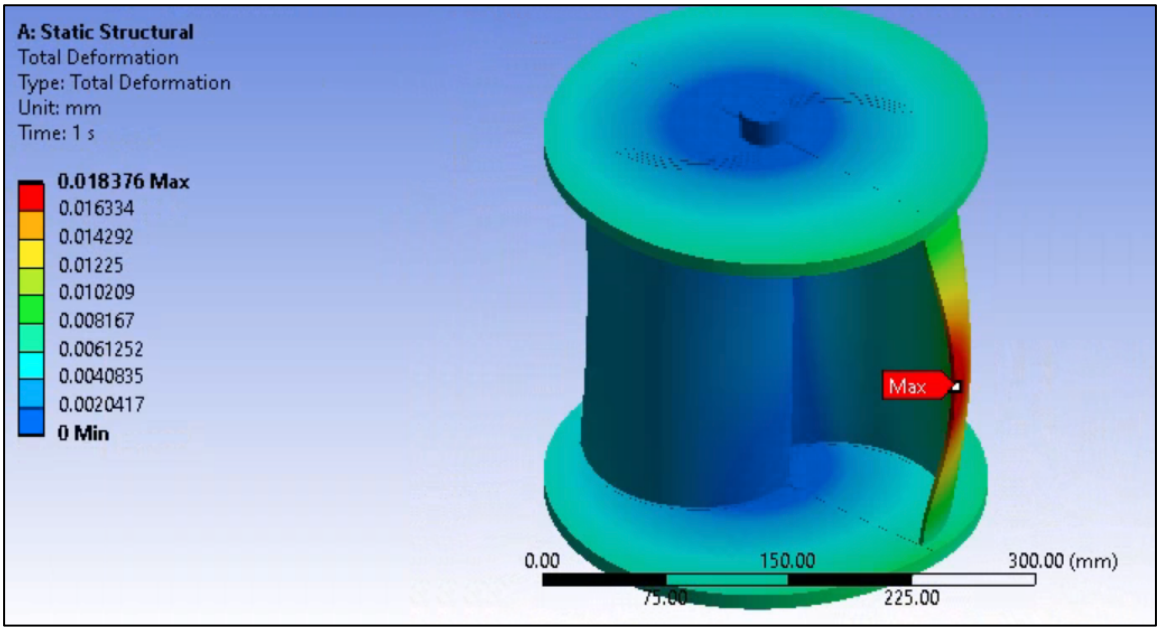

Figure 26 Total deformation results on unchanged model with maximum deformation shown in middle of blade

The maximum deformation in the model was located on the centre of the blade, with a maximum value of 0.018376mm.

Figure 27 shows the results for linearised stress for the first simulation run, down the path.

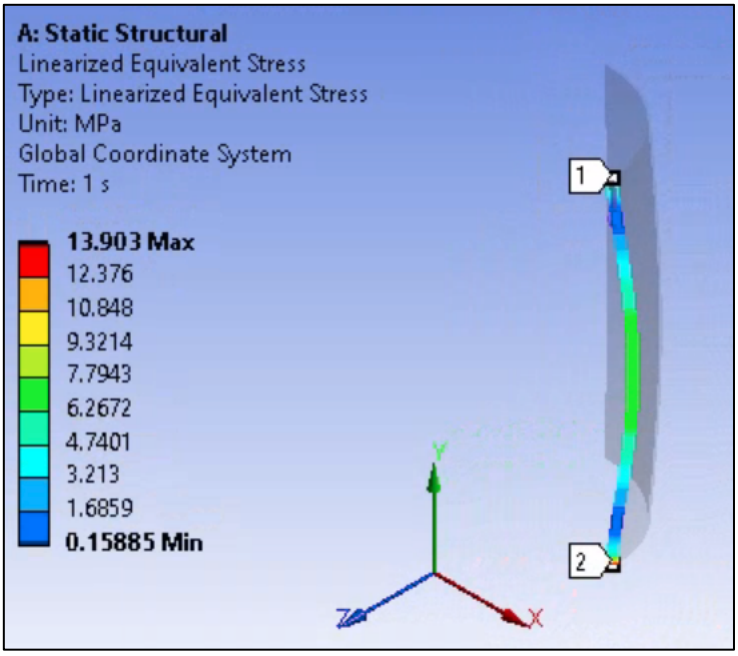

Figure 27 Linearised stress result of unchanged model across path

It can be seen from figure 27 that the maximum stress on this path, which includes the maximum stress on the model, is at the bottom edge of the blade where it connects to the

endplate. This linearised stress allows a graph to be produced of the stress variation down the edge of the blade, as shown in figure 28.

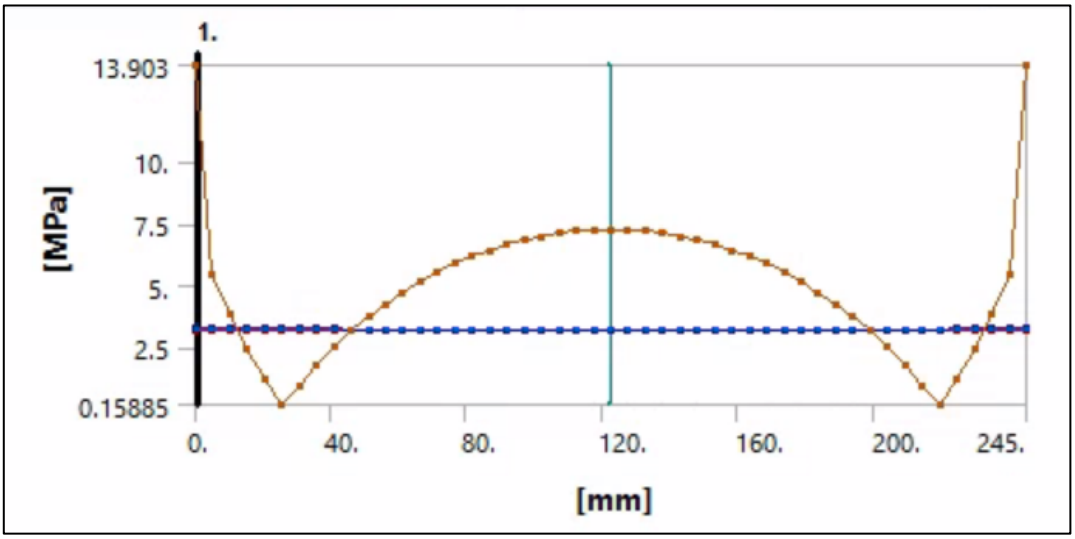

Figure 28 Linearised stress down edge of the blade across path on unchanged model

As can be seen from the figure, the maximum stress occurs at both the top and bottom of the blade and is symmetrical across the horizontal.

The results from this simulation acted as a starting point for the rest of the analysis. The maximum stress, focussed on the blade edge, allows for a direct comparison to be made with further simulations where changes are made to the material of the model. The next section details results acquired from implementing them on the model.

The results from all analyses are shown in table 2.

Table 2 Numerical results from Ansys analysis of all materials chosen

Material	Global Max Deformation	Global Max Stress	Max Stress Blade (linearised)
Units	mm	MPa	MPa
Steel	0.018367	13.903	13.903
GFRP	0.061499	75.352	13.864
CFRP	0.086352	36.367	13.77
Titanium Alloy	0.07563	42.853	13.303

Aluminium Alloy	0.085411	36.791	13.564

All figures for each result for all materials evaluated can be found in Appendix 2.

5.1 Granta Results

This section details the graphs produced from the material analysis in Granta EduPack 2021. The purpose of this analysis was to act as a comparison between the Ansys analysis while keeping other factors in mind, such as price.

Furthermore, analysis of material choices regarding recyclability, or CO2 footprint from recycling was graphed.

Figure 29 shows the graph produced from investigating the Young's modulus of the material versus the price per unit volume of all simulated materials.

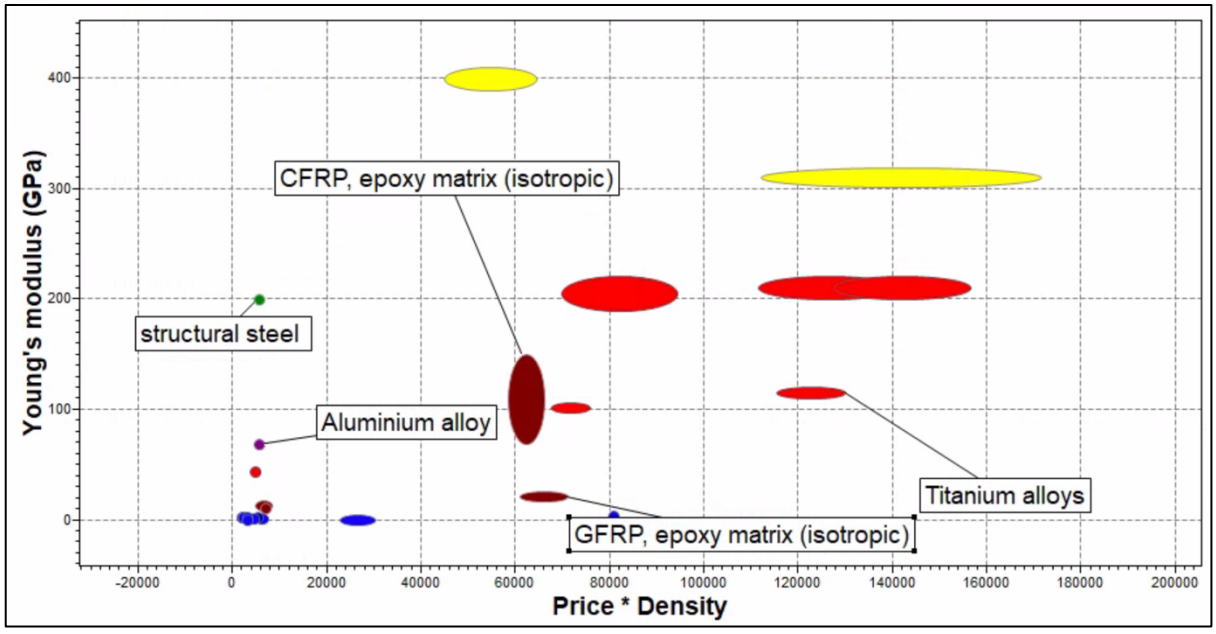

Figure 29 Graph of Young's modulus versus price per unit volume created using Granta EduPack 2021

It is important to note that the graph shows as being plotted against "Price * Density", this is due to the default Price factor in Granta using USD/kg, meaning that for accurate comparison of materials in this case, density was added such that materials could be compared by unit volume.

Furthermore, a graph of fatigue life versus price per unit volume was produced, shown in figure 30.

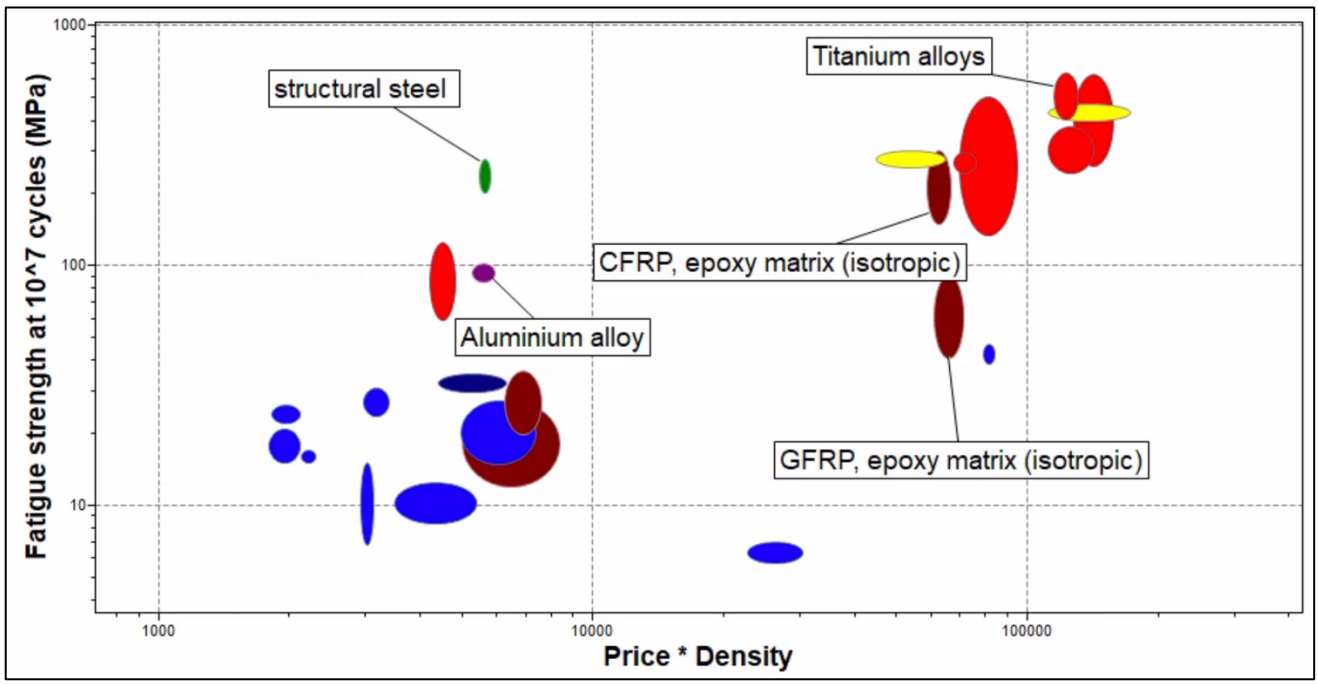

Figure 30 Graph of fatigue life at 10^7 cycles versus price per unit volume created using Granta EduPack 2021

6.0 Discussion

This section details the discussion and analysis of the results provided in section 5.

It is important to note that the global maximum stress on the model varied significantly throughout each iteration. In this case, the maximum stress on the model moved from originally being located on the rotor blades, to being situated on the endplates. Therefore, this proved the importance of the path being inserted on the edge of the blade, as this made results far easier to compare, with variation in stress being less dependent on the geometry of the model, allowing the blades to remain the focus of the analysis.

A reason that could be posed for this wide range in values of global stress could be that when the material was adapted in Ansys, the shaft remained the original steel while the endplates and blades were changed. When the model is loaded into Space Claim, the software considers it to be one solid piece when performing a static structural analysis, meaning that this material change shifts the maximum stress distribution when these materials differ. As can be seen in Appendix 2 the maximum stress in all other iterations after material changes were made

remains in approximately the same location with the main difference being which endplate it occurs on. While this is interesting, not all Savonius turbines include endplates, therefore for further analysis and recommendation will focus on the blades.

From the results steel produces the highest stress on the blade and titanium alloy with the lowest. Steel has the highest Young's modulus of all the materials tested, but a relatively low fatigue strength. When considering the results, it is vital to consider the durability of the materials in water. While steel has a high young's modulus, it would certainly not be a suitable choice for the turbine due to its susceptibility to rusting and corrosion. Therefore, if steel were to be used, it would require coating to allow for better durability.

In comparison titanium alloy produced the lowest stress in the blade, at 13.303 MPa. This was to be expected, as Titanium alloys hold the most desirable material properties, and therefore was expected to produce the smallest stress where the force was applied. This expectation was strengthened by the material analysis in Granta. Titanium alloy consistently outperformed all other materials chosen, in fatigue strength, and is second to steel in young's modulus. However, while this is ultimately positive to the survival of the blades under loading conditions, the other factors which are of interest to producers and designers make Titanium alloy a less desirable option. Arguably most significant of these factors is cost. While the development of tidal turbines is, indeed, a matter of urgency, cost efficiency remains a vital aspect of the design process for producers. Therefore, while Titanium alloy is a strong option in engineering terms, this is unlikely to be brought to fruition in reality.

The comparison between GFRP and CFRP was another aspect of this project which came from a significant number of literature sources comparing the two materials. From the Ansys analysis there was little variation in the maximum linearised stress along the blade edge between CFRP and GFRP, where carbon fibre came out with slightly lower stress. When considering the global maximum stress, which in this case was relevant, GFRP has a significantly higher maximum stress than CFRP. While considering the materials in Granta, both performed almost equally. This was interesting due to the amount of debate in literature between the advantages of each material in comparison. The GFRP produced less deformation than the CFRP, which was expected due to the difference between Young's moduli. In practice this could mean that CFRP would outperform GFRP since in more realistic loading conditions CFRP would be able to withstand the large variations in loading magnitude and direction.

While CFRP and GFRP were lower in price per unit volume as shown in the Granta analysis, they remain expensive options. It could be posed that it is for good reason that these reinforced polymers are often used for turbine blades, but with this analysis that remains, arguably, unproven. It should also be considered, that while CFRP and GFRP durability in salt and fresh water was deemed "excellent" by Granta limitations imposed, the materials reaction to being submerged in water for significant periods of time is less than desirable. When GFRP is submerged in water for long durations of time, the bending strength is reduced and weight is lost, meaning favourable material properties are lost [42].

A further challenge when considering GFRP and CFRP versus other material options such as Aluminium alloy is recyclability. While these composite materials perform strongly, at end of life and decommissioning the materials pose a risk to the environment. This factor is important when considering material options for production, much in the same way that manufacturing of the materials and turbine parts is. To produce renewable energy is undeniably impactful to the fight against climate change, a move to a more circular economy is also vital in all aspects, including technology development.

The results of the analysis on Aluminium alloy show that it produces stresses lower than all but Titanium in the blade. This result shows that aluminium is a strong choice in blade material choice considering all other alternatives, as when also considering the Granta results shows that Aluminium alloy was more cost effective than all other options, other than steel. It is also important to note that Aluminium's behaviour in salt water is favourable to produce turbine blades. Corrosion resistantance to salt water in Aluminium is due to a film of aluminium oxide forming on the surface, making it durable in such conditions [43]. In addition to this, the cost of aluminium is lower than almost all other options, which is beneficial for producers and assists in making the move to renewable energy more profitable and desirable.

The fatigue strength of each material plotted in figure 29 produced further interesting results for analysis. The range of materials analysed could be split into two groups from this graph, with the main differentiating factor being price per unit volume. With Titanium alloy showing the highest fatigue strength, it also was shown, again, to be more expensive than all other options. It is worth noting that this graph demonstrated one of the more pronounced differences between GFRP and CFRP, with CFRP showing much higher fatigue strength. Furthermore, structural steel shows high performance and low cost in this field, with aluminium showing much lower fatigue strength. This was most likely the most pronounced disadvantage of

aluminium alloy throughout the analysis results but would require further testing to fully evaluate. While this was mildly concerning, a conclusion is difficult to take from this result regarding aluminium, as cost of the material remains much lower than composites or titanium.

7.0 Conclusions

The aim of this thesis was to investigate the effect that material choice has on the stress distribution in tidal turbine blades, in the hopes of informing design decision aimed at prolonging turbine lifespan, including durability and end of life behaviour, in the form of recycling.

A model was created using Solidworks and then simulated in Ansys with calculated loading conditions for a set water velocity and density. Following this, model material was adapted to produce results for analysis on how material properties such as Young's modulus and fatigue strength would affect the stresses in the model at an instantaneous interval.

The results from the simulation brought the opportunity for further comparison to data from Granta EduPack software, allowing for a deeper understanding to be built on the full picture of how material choice may affect not only the lifespan of the turbine, but also of the cost.

Aluminium performed well in all categories, proving to show low stress in the blades in the Ansys simulation while also remain cheap, recyclable, and durable in water. When considering which material performed worst, it is difficult to focus on one, due to all having merits in different aspects. Steel performed well but would not be a reliable material choice due to susceptibility of rusting and corrosion when employed without coatings in the ocean.

The results from the Ansys model were largely what were expected depending on the mechanical material properties of each material, with variation in results only diverging when considering the variation in material on individual components rather than the model remaining all one consistent material throughout.

The question posed in various literature sources comparing the merits of CFRP to GFRP, remains only partly answered. In both Ansys and Granta analysis materials performed similarly, and whether it is worth the extra cost of producing blades from carbon fibre is inconclusive from results alone. However, the difference in material properties between the

two materials are vastly different, and it is likely that with further testing with a variety of loading conditions and time spans, the answer to this may become clearer.

While research and development of tidal turbine technology remains in early stages, this analysis provides a starting point for considering alternatives to material choice. With components often produced out of GFRP or other composites, this may not be the optimum choice, and this analysis proves it is worth considering alternate options.

Further work to develop this analysis and deepen knowledge on this subject could take the form of several steps.

The first step in this process would be the strengthening of the simulation model by adding further detail. It could be suggested that it is worth adding multiple loading configurations depending on the varying salinity in different locations worldwide, to begin building a tool that could be a starting point in design processes. The addition of this would affect the forces that are applied to the model and would increase accuracy.

Furthermore, it would be worthwhile building a simulation model that could not only apply loading conditions to the model, but also simulate the effects of prolonged submersion on materials. This would be important in the simulation and further testing of composites currently used for tidal turbines and would assist in the ongoing question as to whether using wind turbines are the starting point for tidal turbine design is the correct approach.

The addition of a dynamic loading model would add value to this research by allowing analysis to include fatigue life of turbine components that are consistently moving and subject to cyclical forces.

Research into coatings on metals will add value to development of models if producers decide on materials like steel for turbine components. This would require analysis on short- and long-term effects of such coatings, which may assist in challenges that arise further down the line for technologies, such as delamination and corrosion. It is possible that coatings may also improve material durability to effects such as cavitation.

Model testing could also take the form of a physical model in testing to compare the accuracy of the simulation, or to highlight factors which may have not been previously considered.

8.0 References

[1] European Commission, "amending Directive (EU) 2018/2001 of the European Parliament and of the Council, Regulation (EU) 2018/1999 of the European Parliament and of the Council and Directive 98/70/EC of the European Parliament and of the Council as regards the promotion of energ," Brussels, 2021.

[2] The Scottish Government, "Update to the Climate Change Plan 2018-2032," The Scottish Government , Edinburgh, 2020.

[3] Scottish Renewable, "Statistics - Energy Consumption by Sector," tictoc, 2022. [Online]. Available: https://www.scottishrenewables.com/our-industry/statistics. [Accessed 15 August 2022].

[4] K. R. Rahaman and Q. K. Hassan, "Prospects and Challenges of Wind Energy: A Comprehensive Anatomy," in *Proceedings of the International Conference on Mechanical Engineering 2011*, Bangladesh, 2011.

[5] The Crown Estate, "UK Wave and Tidal Key Resource Areas Project," The Crown Estate, London, 2012.

[6] The European Marine Energy Centre Ltd, "EMEC - About Us," Shaw, 2022. [Online]. Available: https://www.emec.org.uk/about-us/. [Accessed 15 August 2022].

[7] C. Glennon, W. Finnegan, N. Kaufmann, P. Meier, Y. Jiang, R. Starzmann and J. Goggins, "Tidal stream to mainstream: mechanical testing of composite tidal stream blades to de-risk operational design life," *Journal of Ocean Engineering and Marine Energy,* vol. 8, pp. 163-182, 2022.

[8] A. Owen, "Chapter 16 - Tidal Current Energy: Origins and Challenges," in *Future Energy Second Edition*, Elsevier Ltd, 2014, pp. 335-356.

[9] P. Webb, Introduction to Oceanography, Rebus Community, 2019.

[10] National Ocean Service, "Tides and Water Levels," n.d.. [Online]. Available: https://rwu.pressbooks.pub/webboceanography/chapter/11-3-tide-classification/. [Accessed 25 July 2022].

[11] Z. Zhou, F. Scuiller, J. Frederic Charpentier, M. Benbouzid and T. Tang, "An Up-to-Date Review of Large Marine Tidal Current Turbine Technologies," in *Internation Power Electronics and Application Conference and Exposition*, 2014.

[12] R. Pelc and R. M. Fujita, "Renewable energy from the ocean," *Marine Policy,* vol. 26, no. 6, pp. 471-479, 2002.

[13] M. Esteban and D. Leary, "Current developments and future prospects of offshore wind and ocean energy," *Applied Energy,* vol. 90, no. 1, pp. 128-136, 2012.

[14] C. Frost, C. Morris, A. Mason-Jones, D. O'Doherty and T. O'Doherty, "The effect of tidal flow directionality on tidal turbine performance characteristics," *Renewable Energy,* vol. 78, pp. 609-620, 2015.

[15] M. Benbazoud, J. Astolfi, B. Seddik, J.-F. Charpentier, M. Machmoum, T. Maitre and D. Roye, "Concepts, Modeling and Control of Tidal Turbines," *Marine Renewable Energy Handbook,* pp. 219-278, 2013.

[16] S. Abdel Aleem, A. Zobaa and A. Ibrahim, Mathematical Analysis of the Turbine Coefficient of Performance for Tidal Stream Turbines, 2014.

[17] R. Kempener and F. Neumann, "Tidal Energy - Technology Brief," International Renewable Energy Agency, 2014.

[18] C. Jiang, X. Shu, J. Chen, L. Bao and Y. Xu, "Research on Blade Design of Lift–Drag-Composite Tidal-Energy Turbine at Low Flow Velocity," *Energies,* vol. 14, 2021.

[19] D. Satrio, I. Utama and Mukhtasor, "Vertical Axis Tidal Current Turbine: Advantages and Challenges Review," *Ocean, Mechanical and Aerospace - Science and Engineering,* vol. 3, pp. 64-71, 2016.

[20] P. Ouro and T. Stoesser, "Impact of Environmental Turbulence on the Performance and Loadings of a Tidal Stream Turbine," *Flow Turbulence Combust,* vol. 102, pp. 613-639, 2019.

[21] J. Khan and T. Iqbal, "River current energy conversion systems: Progress, prospects and challenges," *Renewable and Sustainable Energy Reviews,* vol. 12, pp. 2177-2193, 2008.

[22] B. L. Kirke and L. Lazauskas, "Limitations of fixed pitch Darrieus hydrokinetic turbines and the challenge of variable pitch," *Renewable Energy,* vol. 36, no. 3, pp. 893-897, 2011.

[23] M. Khan, G. Bhuyan, M. Iqbal and J. Quaicoe, "Hydrokinetic energy conversion systems and assessment of horizontal and vertical axis turbines for river and tidal applications: A technology status review," *Applied Energy,* vol. 86, no. 10, pp. 1823-1835, 2009.

[24] F. Wenehenubun, A. Saputra and H. Sutanto, "An experimental study on the performance of Savonius wind turbines related with the number of blades," *Energy Procedia,* vol. 68, pp. 297-304, 2015.

[25] A. Kumar and R. Saini, "Performance analysis of a Savonius hydrokinetic turbine having twisted blades," *Renewable Energy,* vol. 108, pp. 502-522, 2017.

[26] A. Kumar and R. Saini, "Performance analysis of a Savonius hydrokinetic turbine having twisted blades," in *2015 International Conference on Recent Developments in Control, Automation and Power Engineering*, Noida, 2015.

[27] J.-L. Menet and R. Tassio, Static and dynamic study of a conventional Savonius rotor using a numerical simulation, 2013.

[28] Blue Energy Canada Inc, "Blue Energy - Tidal Bridge," [Online]. Available: http://www.bluenergy.com/technology_method_tidal_bridge.html. [Accessed 15 July 2022].

[29] Xi Engineering , "Fatigue and Tidal Energy," 19 June 2019. [Online]. Available: https://xiengineering.com/tidal-fatigue/. [Accessed 27 July 2022].

[30] P. Galloway, "Performance quantification of tidal turbines subjected to dynamic loading," University of Southampton- Faculty of Engineering and Environment , 2013.

[31] G. McCann, W. M. Batten and A. S. Bahaj, "Experimental verifications of numerical predictions for the hydrodynamic performance of horizontal axis marine current turbines," *Renewable Energy,* vol. 32, no. 15, pp. 2479-2490, 2007.

[32] R. B. Barber and M. R. Motley, "Cavitating response of passively controlled tidal turbines," *Journal of Fluids and Structures,* vol. 66, pp. 462-475, 2016.

[33] P. Kumar and R. Saini, "Study of cavitation in hydro turbines—A review," *Renewable and Sustainable Energy Reviews ,* vol. 14, no. 1, pp. 374-383, 2010.

[34] C. R. Kennedy, V. Jaksic, S. B. Leen and C. M. Bradaigh, "Fatigue life of pitch- and stall-regulated composite tidal turbine blades," *Renewable Energy,* vol. 2018, pp. 688-699, 121.

[35] G. S. Galloway, V. M. Catterson, C. Love, A. Robb and T. Fay, "Fatigue life of pitch- and stall-regulated composite tidal turbine blades," *Fatigue life of pitch- and stall-regulated composite tidal turbine blades,* vol. 50, no. 4, pp. 1252-1259, 2020.

[36] G. Nehls, "European partnership drives forward novel process development for GFRP recycling," Composites World , 6 November 2021. [Online]. Available: https://www.compositesworld.com/news/european-partnership-drive-forward-novel-process-development-for-gfrp-recycling. [Accessed 22 August 2022].

[37] D. Kumar and S. Sarkar, "Numerical investigation of hydraulic load and stress induced in Savonius hydrokinetic turbine with the effects of augmentation techniques through fluid-structure interaction analysis," *Energies,* vol. 116, pp. 609-618, 2016.

[38] N. Hall, "NASA - The Drag Equation," NASA, 13 May 2021. [Online]. Available: https://www.grc.nasa.gov/www/k-12/airplane/drageq.html. [Accessed 1 August 2022].

[39] I. S. Hoerner, Fluid-Dynamic Drag, Bakersfield: Hoerner Fluid Dynamics, 1965.

[40] F. Rubino, A. Nistico, F. Tucci and P. Carlone, "Marine Application of Fiber Reinforced Composites: A Review," *Journal of Marine Science and Engineering ,* vol. 8, no. 26, 2020.

[41] P. Alam, C. Robert and C. M. BRadaigh, "Tidal turbine blade composites - A review on the effects of hygrothermal aging on the properties of CFRP," *Composites Part B: Engineering,* vol. 149, pp. 248-259, 2018.

[42] I. Nishizaki and S. Meiarashi, "Long-Term Deterioration of GFRP in Water and Moist Environment," *Journal of Composites for Construction,* vol. 6, 2002.

[43] D. Feron, Corrosion Behaviour of Aluminium in Marine Environments, Elesevier, 2007.

9.0 Appendices

9.1 Appendix 1

Table of mesh convergence study and figures of a couple of coarser meshes

No. Elements	Max Stress MPa
1573	7.0775
4520	8.2912
17822	11.311
30296	12.199
52305	13.112
77325	13.903
88501	14.012

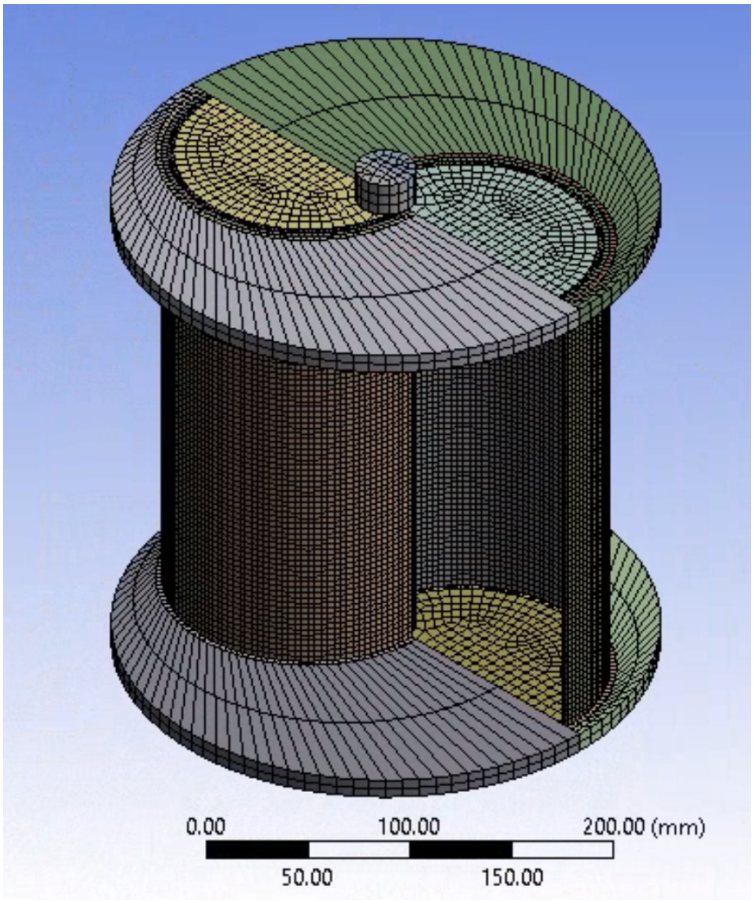

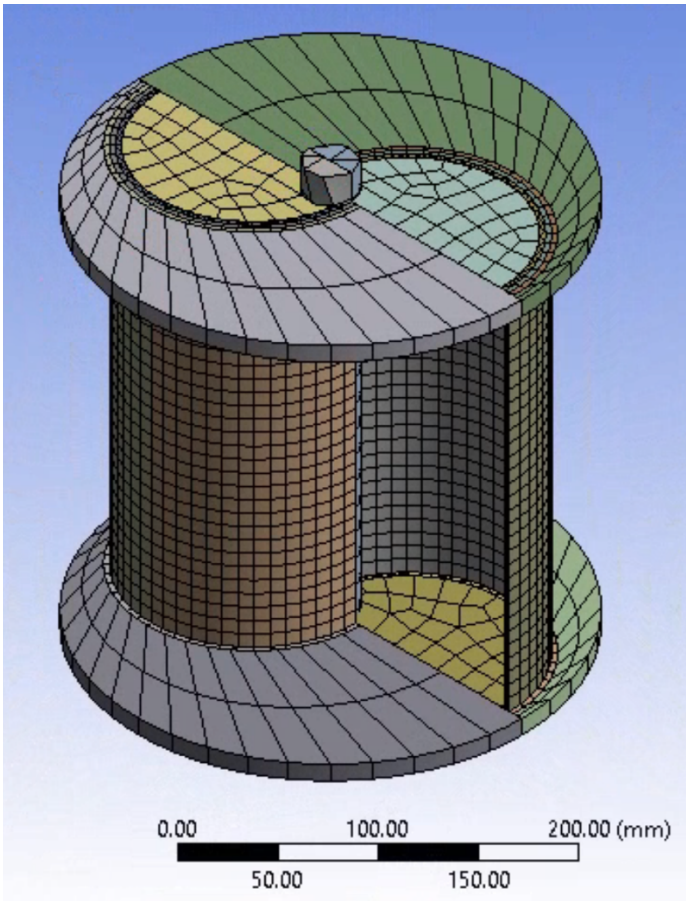
0.00
100.00
200.00 (mm)
50.00
150.00

9.2 Appendix 2

CFRP

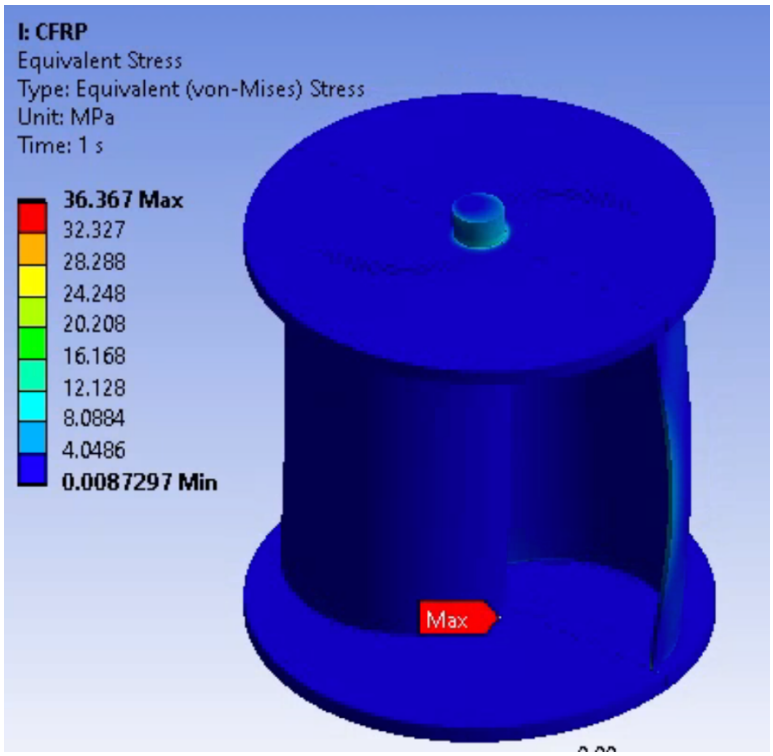

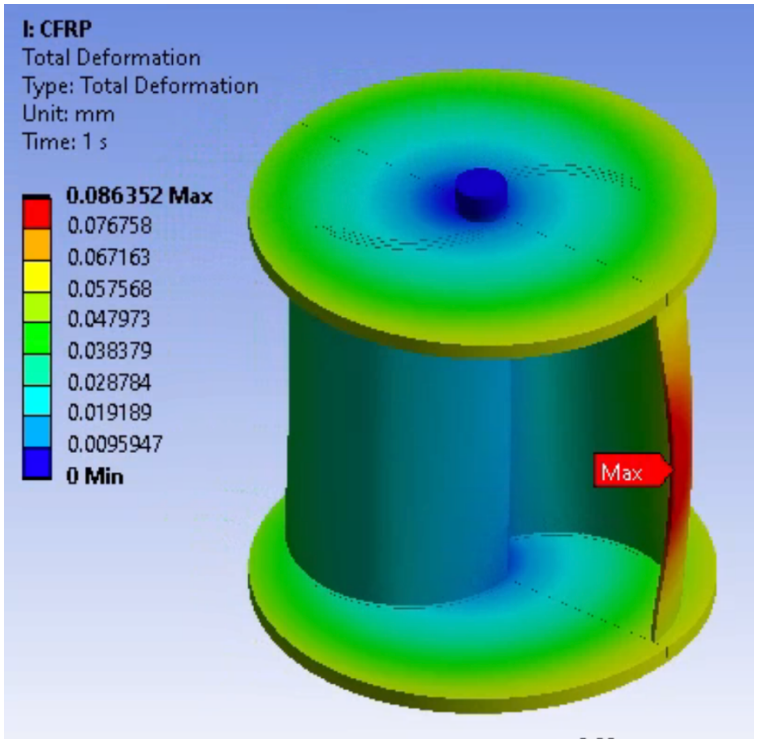

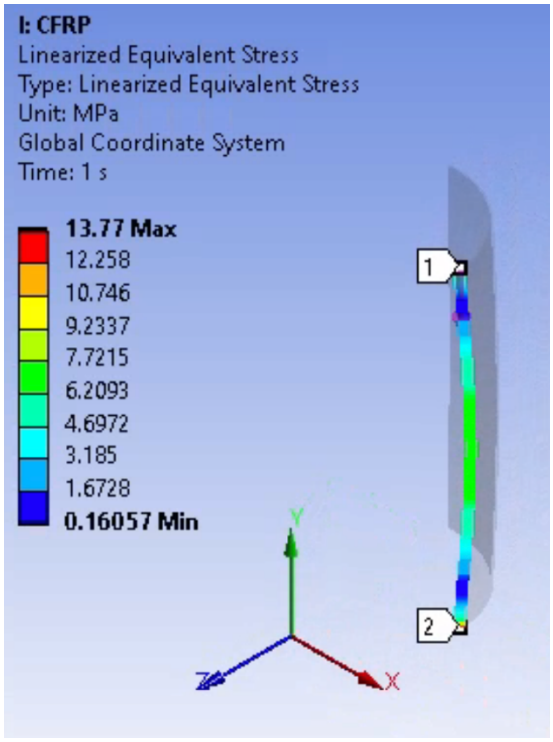
I: CFRP
Linearized Equivalent Stress
Type: Linearized Equivalent Stress
Unit: MPa
Global Coordinate System
Time: 1 s
13.77 Max
12.258
10.746
9.2337
7.7215
6.2093
4.6972
3.185
1.6728
0.16057 Min
1
2
Y
Z
X

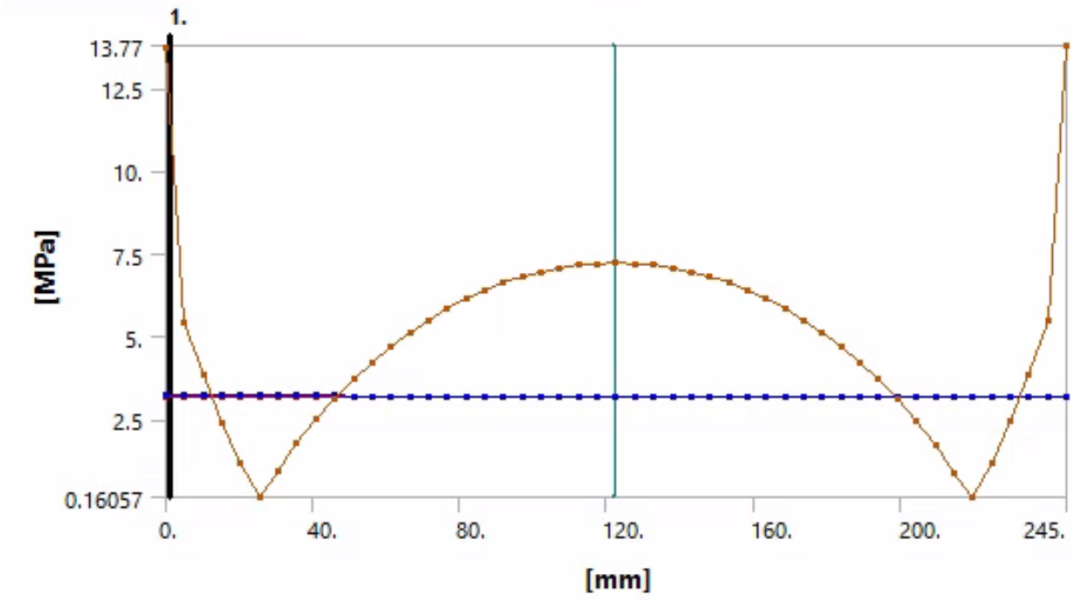
1.
13.77
12.5
10.
7.5
5.
2.5
0.16057
[MPa]
0.
40.
80.
120.
160.
200.
245.
[mm]

GFRP

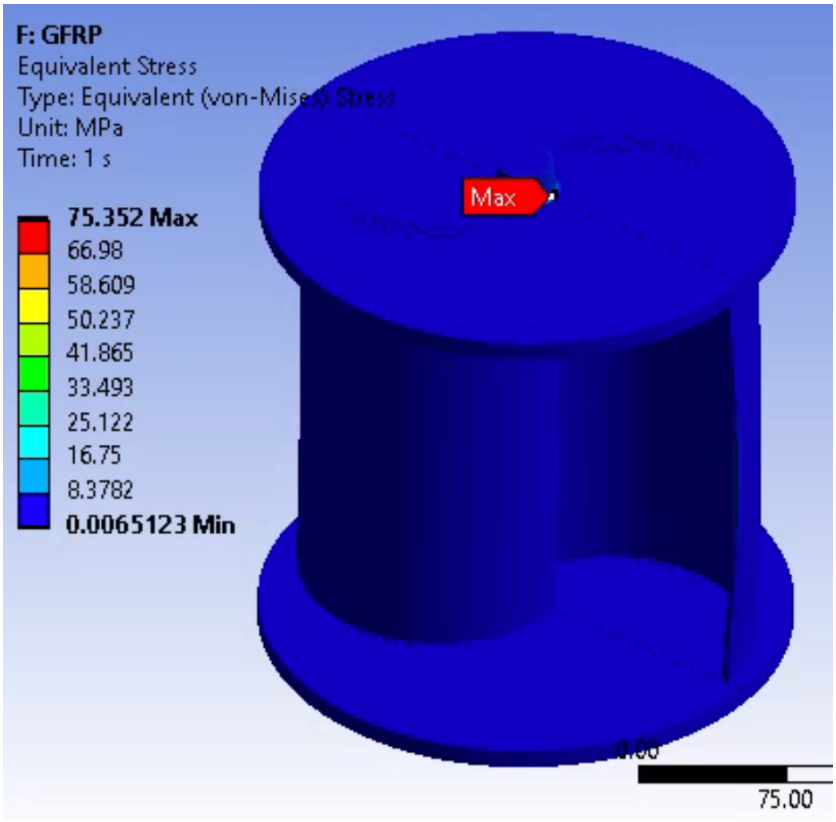
F: GFRP
Equivalent Stress
Type: Equivalent (von-Mises) Stress
Unit: MPa
Time: 1 s
75.352 Max
66.98
58.609
50.237
41.865
33.493
25.122
16.75
8.3782
0.0065123 Min
Max
0.00
75.00

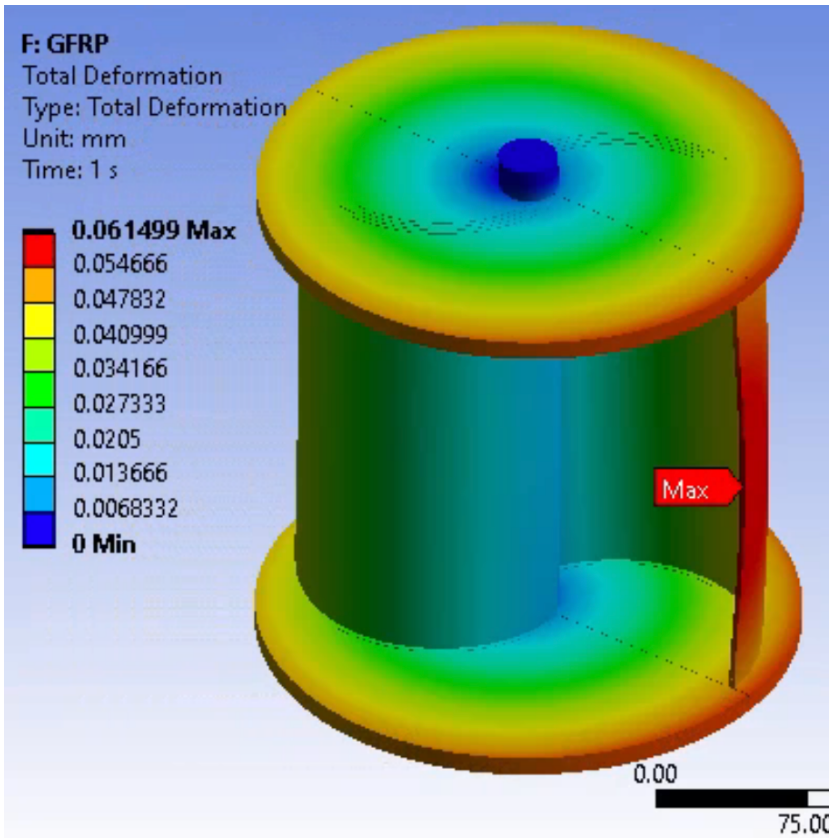
F: GFRP
Total Deformation
Type: Total Deformation
Unit: mm
Time: 1 s
0.061499 Max
0.054666
0.047832
0.040999
0.034166
0.027333
0.0205
0.013666
0.0068332
0 Min
Max
0.00
75.00

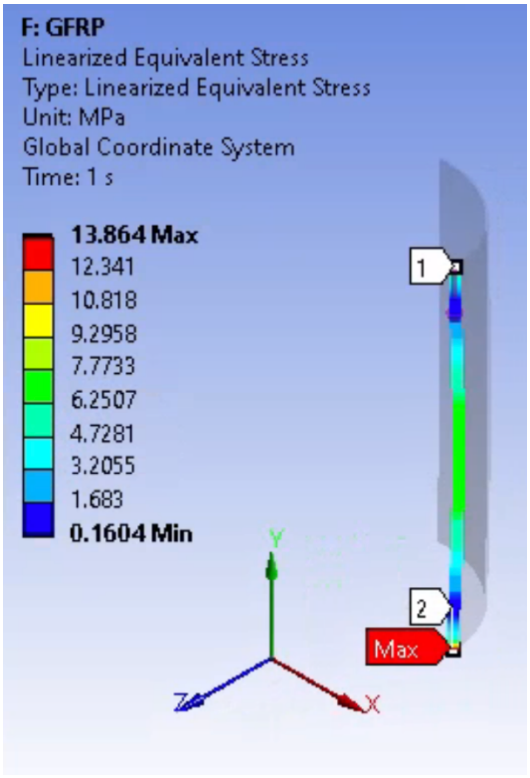
F: GFRP
Linearized Equivalent Stress
Type: Linearized Equivalent Stress
Unit: MPa
Global Coordinate System
Time: 1 s
13.864 Max
12.341
10.818
9.2958
7.7733
6.2507
4.7281
3.2055
1.683
0.1604 Min
1
2
Max
Y
Z
X

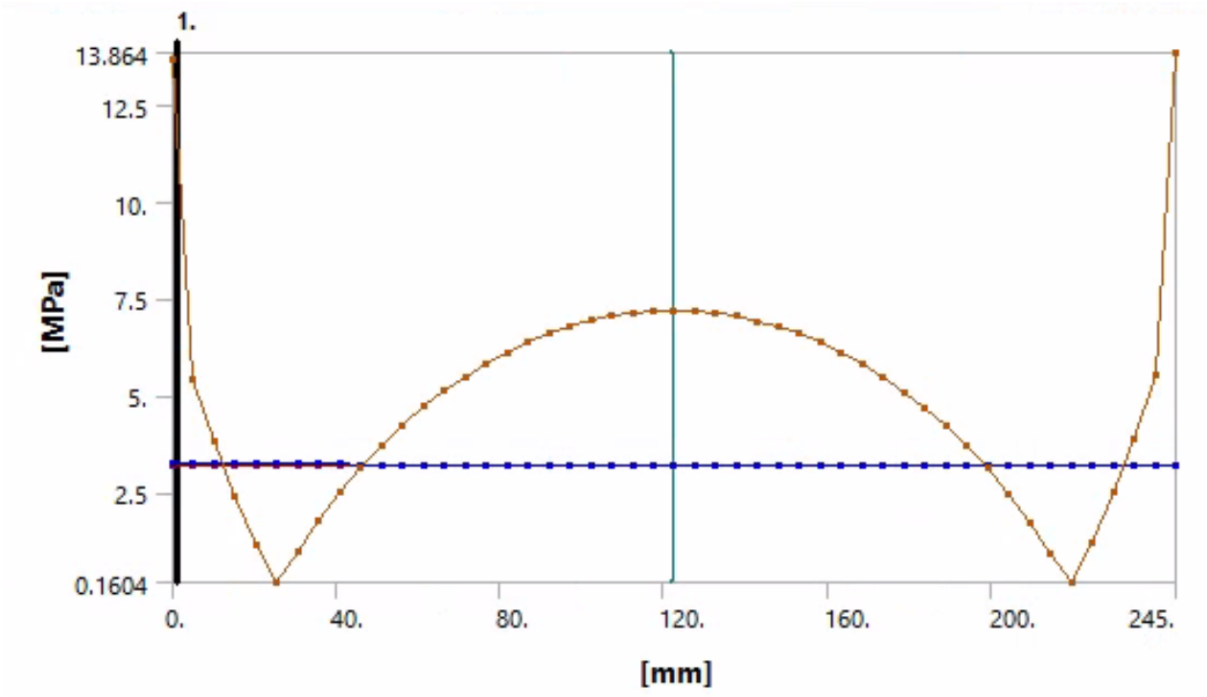
1.
13.864
12.5
10.
7.5
5.
2.5
0.1604
[MPa]
0.
40.
80.
120.
160.
200.
245.
[mm]

Titanium Alloy

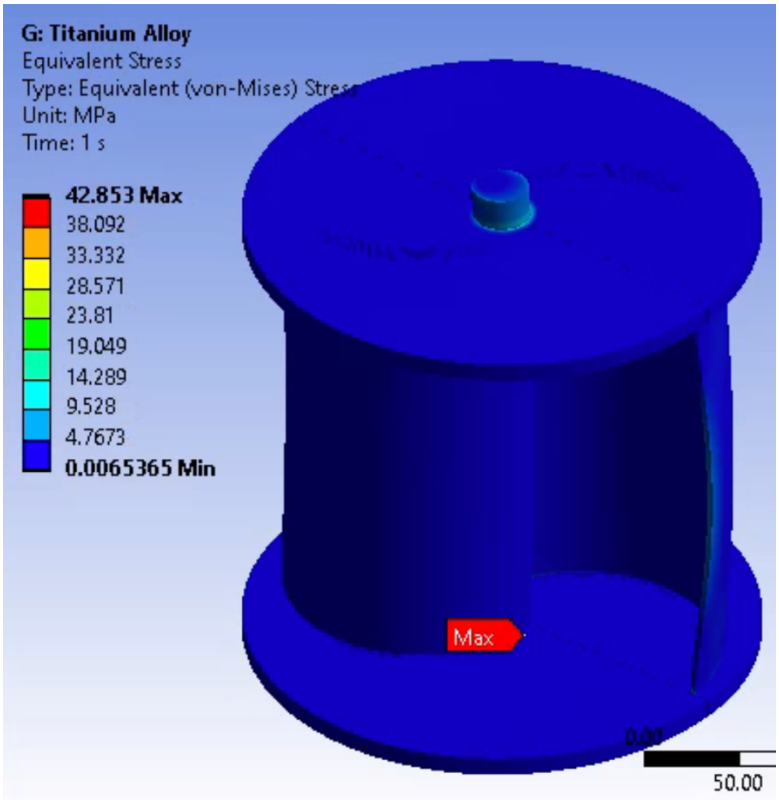

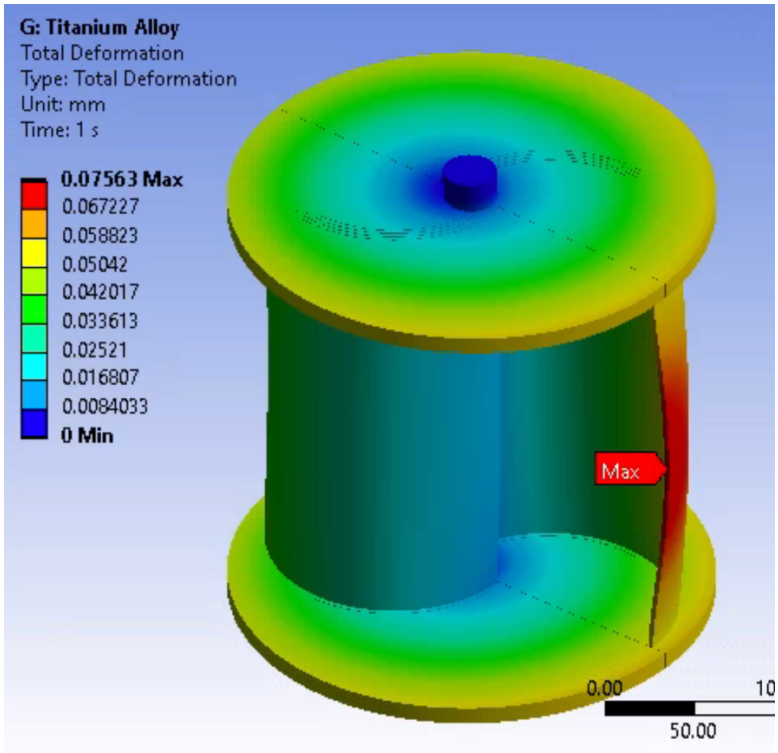

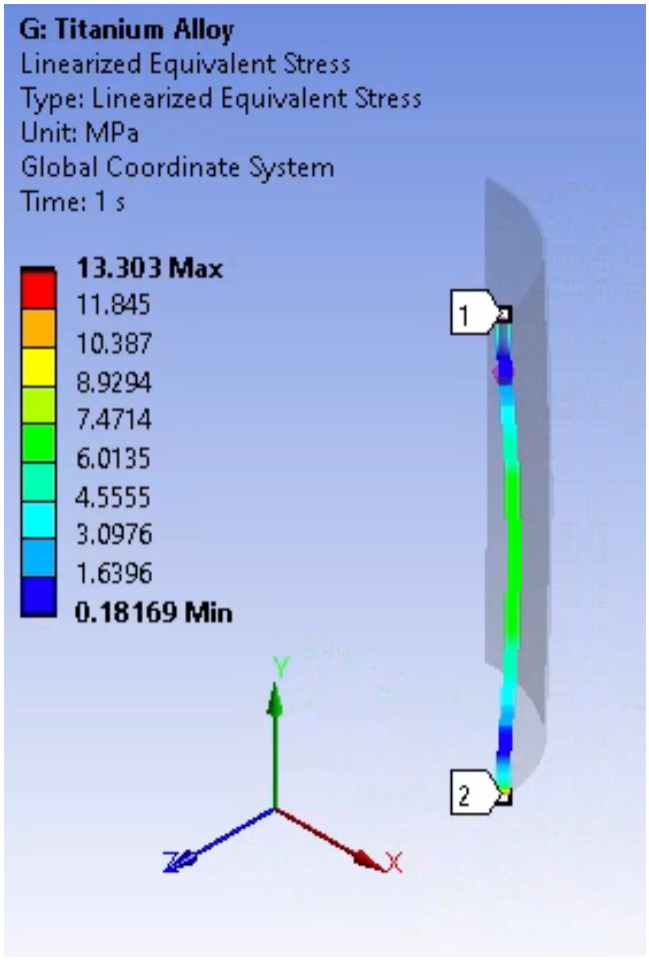
G: Titanium Alloy
Linearized Equivalent Stress
Type: Linearized Equivalent Stress
Unit: MPa
Global Coordinate System
Time: 1 s
13.303 Max
11.845
10.387
8.9294
7.4714
6.0135
4.5555
3.0976
1.6396
0.18169 Min
1
2
Y
Z
X

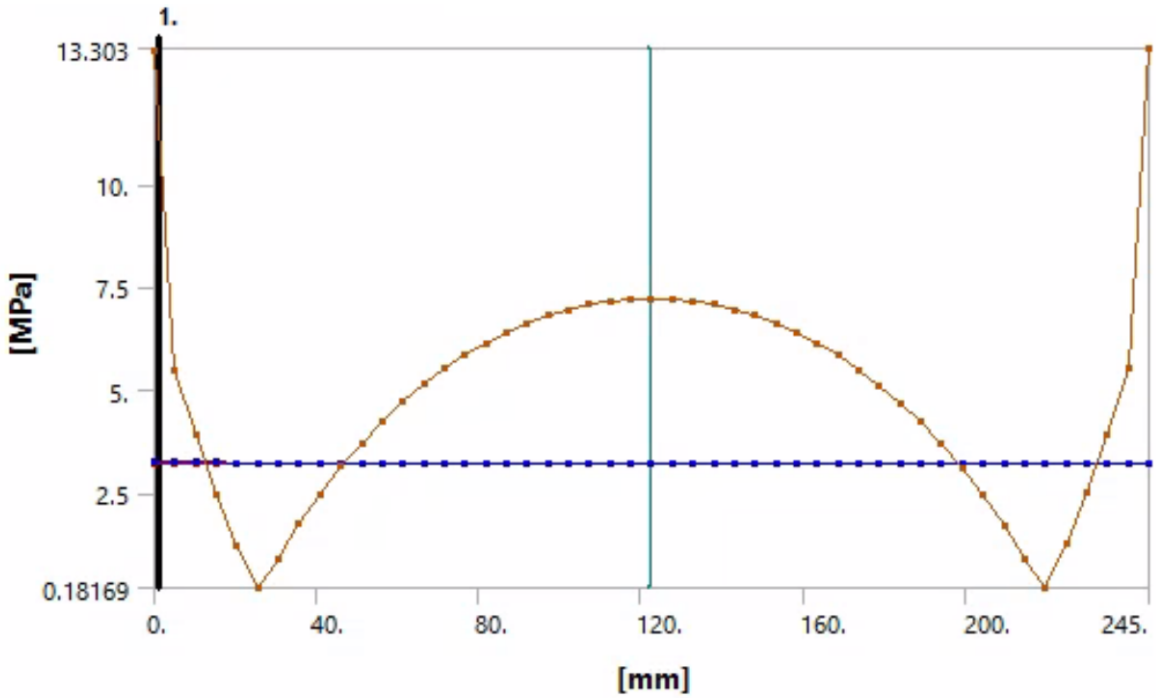
1.
13.303
10.
7.5
5.
2.5
0.18169
[MPa]
0.
40.
80.
120.
160.
200.
245.
[mm]

Aluminium Alloy

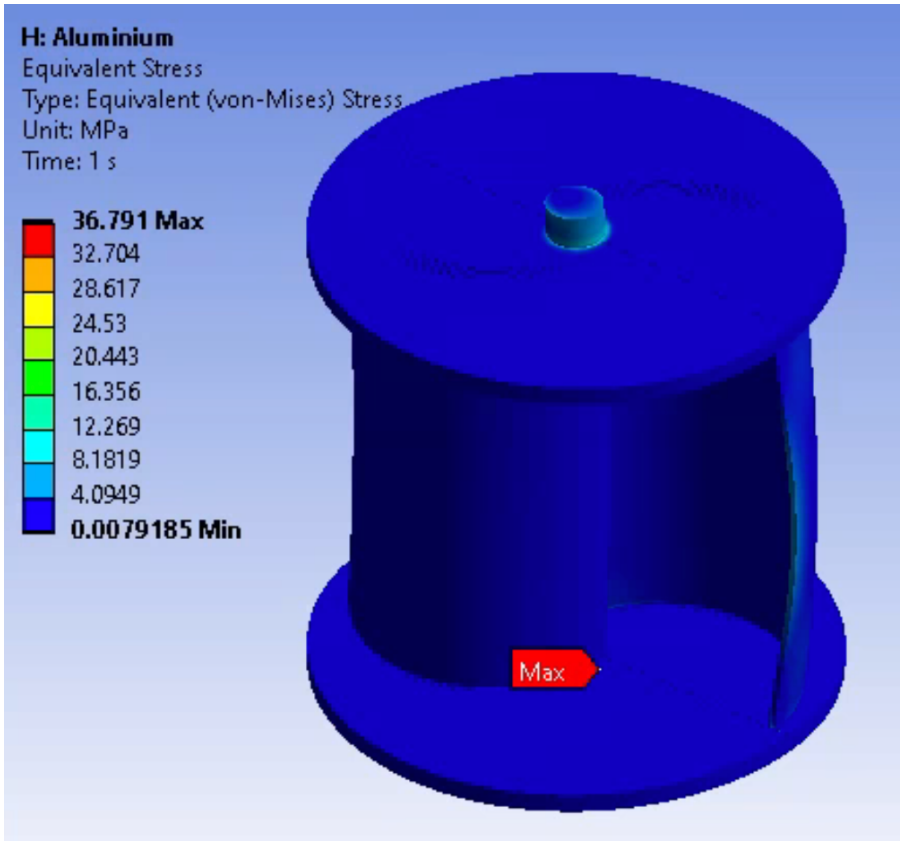

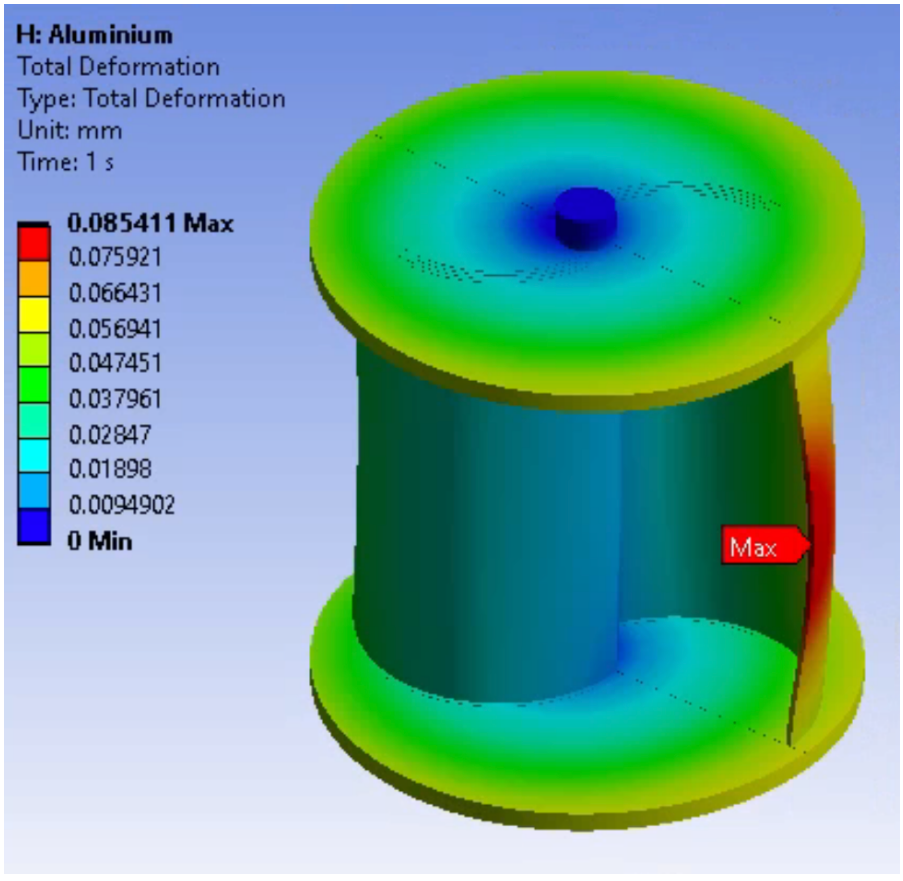

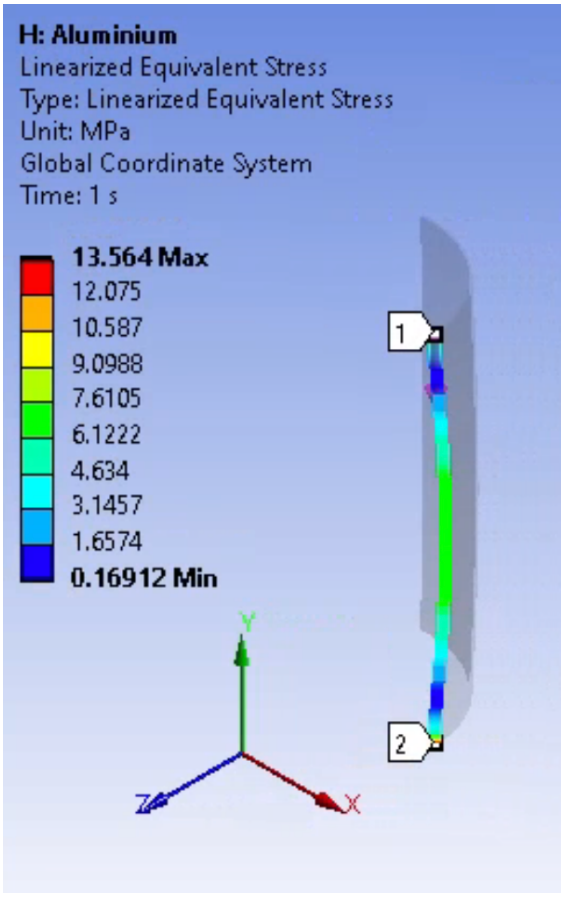
H: Aluminium
Linearized Equivalent Stress
Type: Linearized Equivalent Stress
Unit: MPa
Global Coordinate System
Time: 1 s
13.564 Max
12.075
10.587
9.0988
7.6105
6.1222
4.634
3.1457
1.6574
0.16912 Min
1
2
Y
Z
X

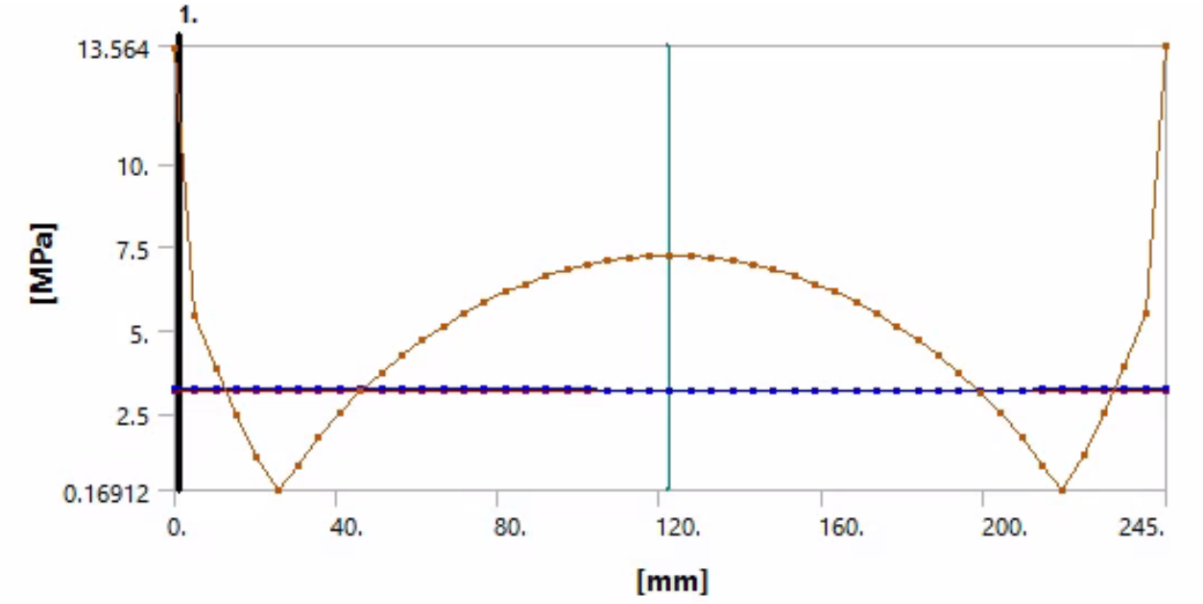
1.
13.564
10.
7.5
5.
2.5
0.16912
[MPa]
0.
40.
80.
120.
160.
200.
245.
[mm]